PULSED FIELD GALVANOMAGNETIC MEASUREMENTS ON ZINC OXIDE

By

WALTER CLAUD RHODES, JR.

Bachelor of Science
Central State University
Edmond, Oklahoma
1957

Master of Science
Oklahoma State University
Stillwater, Oklahoma
1968

Submitted to the Faculty of the
Graduate College of the
Oklahoma State University
in partial fulfillment of
the requirements for
the Degree of
DOCTOR OF PHILOSOPHY
July, 1973

PULSED FIELD GALVANOMAGNETIC
MEASUREMENTS ON ZINC OXIDE

Thesis Approved:

William J. Lewis
Thesis Adviser

Delleth K. Rutledge

Tom E. Moore

John N. Shelton

D. D. Durham
Dean of the Graduate College

PREFACE

This study is concerned with the electronic conduction properties in the semiconductor zinc oxide (ZnO). The primary objective is to contribute to the understanding of the conduction band edge symmetries and band structure of ZnO. Measurements of magnetoresistance and Hall effect were made at room temperature using pulsed magnetic fields up to 200 kilogauss on single-crystal specimens of ZnO.

The measurements represent a more systematic approach and were made at field strengths an order of magnitude greater than those previously used in the study of ZnO. The results of the measurements are compared with and analyzed in terms of current magnetoresistance theories.

I express my appreciation for the assistance and guidance given me by the following members of the physics staff: My adviser, Dr. W. J. Leivo, for his patience and counsel on this problem; Dr. W. A. Sibley, for encouragement, equipment and financial aid to support this study; my advisory committee for their time and interest, especially Dr. D. L. Rutledge, who was my first physics teacher and sparked my interest in physics; Dr. E. E. Lafon, for assistance with computer programs; and to the Physics and Chemistry shop personnel who did a good job constructing much of the equipment used in this study.

Finally, special gratitude is expressed to my wife, Phyllis, our son, Larry, and our daughter, Beverly, for their understanding, encouragement, and many sacrifices.

TABLE OF CONTENTS

LIST OF TABLES

LIST OF FIGURES

CHAPTER I

INTRODUCTION

Statement of the Problem

The purpose of this study is to contribute to the knowledge and understanding of electronic conduction in a semiconductor. The accepted explanation for electronic conduction is based on the quantum theory of solids with the associated concepts of energy bands, band gaps, Fermi surfaces, effective masses, and holes. This study is specifically addressed to the determination of the conduction band edge symmetry in the semiconductor zinc oxide (ZnO).

When electronic conduction is studied experimentally in the laboratory, galvanomagnetic effects are readily observed. The term "galvanomagnetic" refers to the additional electric fields produced when a current carrying conductor is immersed in a magnetic field. The most well known is the Hall effect (1). In the Hall effect there is produced an electric field which is perpendicular to both the magnetic field and the current. The magnetoresistance effect is the production of an electric field which is parallel to the current when a magnetic field is applied to the conductor. The magnitude and directional characteristics of these

effects can be calculated if one knows the energy band structure and parameters for the material being studied. Conversely, if one experimentally measures these effects, some properties of the band structure can be inferred.

Measurements of magnetoresistance effects have been very useful in giving initial equalitative information about the band edge symmetries and band structures of nearly all semiconductors of interest. The application of this effect to study germanium and silicon is well documented (2) (3). A good review article for magnetoresistance of the III-V compounds is given by W. A. Becker (4), and a review of the known properties and band structure studies of the II-VI compounds is given by Brian Ray (5). ZnO is a II-VI compound; however, only a limited number of measurements have been made on single crystal material. The purpose of this study is, therefore, to contribute to the knowledge concerning the conduction band edge of ZnO by making a systematic study of the galvanomagnetic effects in pulsed magnetic fields up to 200 kilogauss.

Zinc Oxide

ZnO crystalizes with a wurtzite structure having lattice constants, a = 3.24 Å and c = 5.19 Å. The optical band gap is approximately 3.2 eV at room temperature. The space group is C_{6V}^4 and the corresponding point group is C_{6V}. The first Brillouin zone is a right hexagonal prism (6).

ZnO is a compound that has been known since the Bronze age (7). It has many industrial applications and is used in paint, in medical ointment, as a chemical catalyst, and as a luminescent material for television screens. The electrical and optical properties have been extensively studied in recent years. Many of the published articles contain a comprehensive review of these studies (7) (8) (9). Most investigators agree that "as grown" single crystals of ZnO is n-type with the primary donors being interstitial zinc ions.

There have been several Hall effect studies made on both sintered powdered samples and single crystal samples (10) (11) (12) (13). The most significant, with reference to this study, are those made by Hutson (12) (13). Hutson's study was made on single crystals grown in the form of hexagonal needles with the 'C' crystallographic direction parallel to the long axis of the needle. The average measured value of the Hall mobility, μ_H, at 300°K was found to be 180 cm^2 per volt second. Good agreement between theory and experiment in the temperature range 200°K to 600°K was obtained by assuming that the total mobility was due almost entirely to lattice scattering; and that $\mu_L = \mu_a \mu_o/(\mu_a + \mu_o)$ where the subscript, a, refers to acoustical mode scattering and, o, refers to optical mode scattering. At 300°K the ratio, μ_a/μ_o, appears to be 1.7.

Hutson also made magnetoresistance measurements at fields up to a maximum of 15.6 kilogauss and at temperatures of 77°K and 300°K. Both transverse and longitudinal

magnetoresistance exhibited a B^2 dependence over the magnetic field range. The ratio of transverse to longitudinal magnetoresistance at $300^{\circ}K$ was approximately 6. The most significant feature of these magnetoresistance measurements was the fact that the longitudinal magnetoresistance does not vanish for current along the c-axis. This fact, in conjunction with other appropriate experimental evidence, led Hutson to propose a simple-many-valley model for the conduction band of ZnO. It was further stated that a minimum of 12 valleys was needed to meet the symmetry requirements of the crystal.

Hutson combined the results of the magnetoresistance measurements with measurements of electrical conductivity, Hall effect, and thermoelectric power to derive a value of 0.27m for the conduction band effective mass. The theories and assumptions were not completely satisfactory, however, since they did not yield the proper temperature dependence for thermoelectric power. In a later paper, Hutson considers the problem further (14). Inclusion of two piezoelectric scattering mechanisms and an effective electron mass of about 0.32m, derived from other experiments, provided a model for phonon drag in ZnO which agrees with the temperature dependence for the data within the limits of experimental error. This revised theory, along with the experiments in optical absorption in ZnO by Dietz et al. (15), caused Hutson to revise his model for the conduction band of ZnO. The following quotation is taken from Hutson's

paper: "We believe that the semiconducting properties of ZnO may be properly understood with a nearly isotropic conduction band mass of approximately 0.32m (including polaron effects) for a minimum at k = 0. The longitudinal magnetoresistance measured along the hexagonal axis may be due to slight warping of the energy surface due to higher bands."

The above stated concept of the conduction band in ZnO was held at the time this present study began. In view of the limited experimental measurements of magnetoresistance in ZnO to date and the success of magnetoresistance studies of other semiconductors in yielding band structure data, the present systematic study of galvanomagnetic effects in ZnO in fields up to 200 kilogauss was undertaken.

Galvanomagnetic Measurements

The measurement and analysis of galvanomagnetic effects is done using a phenomenological approach. The phenomenological theory has been developed by several authors. This present study has followed the example of Smith, Janak, and Adler (16) and Beer (3) in applying the phenomenological approach to the problem as outlined in the paragraphs to follow.

For an anisotropic isothermal solid, the electrical conductivity is a tensor and is defined by the relation

$$J_i = \sigma_{ij} E_j \qquad (1)$$

where J_i is a component of current density and E_j is a component of electric field. The subscripts refer to

components along a set of cartesian coordinates in the solid. (Note: The Einstein summation convention is used here and throughout the report. The convention states that in a term consisting of a product of factors with subscripts and superscripts any repeated indices are to be summed over their entire range. Greek letters are used for repeated indices when summation is not intended.) Equation (1) is a linear relation i.e. the electrical conductivity tensor is independent of current density or electric field. The case we consider here is an isothermal solid with no temperature gradients; therefore, the conductivity can depend only on temperature, T, and magnetic flux density, B. Following the example previously cited, the conductivity is expanded in powers of B:

$$\sigma_{ij}(\vec{B}) = \sigma_{ij} + \sigma_{ijk}B_k + \sigma_{ijkl}B_kB_l + \cdots, \tag{2}$$

where

$$\sigma_{ijk} = [\partial\sigma_{ij}(\vec{B})/\partial B_k]_{B=0}, \tag{3}$$

$$\sigma_{ijkl} = \tfrac{1}{2}[\partial^2\sigma_{ij}(\vec{B})/\partial B_k\partial B_l]_{B=0}, \tag{4}$$

and σ_{ij} is the zero magnetic-field conductivity. The expansion given by equation (2) is valid provided that the relation

$$\mu B \equiv \omega\tau < 1, \tag{5}$$

where μ is the carrier drift mobility, ω is the cyclotron frequency, and τ is the relaxation time. The cyclotron frequency is defined by the relation

$$\omega = eB/m^* \tag{6}$$

where e is the charge of the carrier in a magnetic field B

and m* is the effective mass of the carrier in the periodic potential of the solid. The relationship of equation (5) is satisfied for the measurements made on ZnO in this study.

The electrical transport effects can also be expressed in terms of the electrical tensor $\underset{\sim}{\rho}(\vec{B})$ by the relation

$$E_i = \rho_{ij}(\vec{B})J_j. \tag{7}$$

The resistivity tensor $\rho_{ij}(\vec{B})$ is expanded in powers of B in the same manner as was the conductivity to yield

$$\rho_{ij}(\vec{B}) = \rho_{ij} + \rho_{ijk}B_k + \rho_{ijkl}B_kB_l + \cdots \tag{8}$$

where

$$\rho_{ijk} = [\partial\rho_{ij}(\vec{B})/\partial B_k]_{B=0}\ , \tag{9}$$

$$\rho_{ijkl} = \frac{1}{2!}[\partial^2\rho_{ij}(\vec{B})/\partial B_k\partial B_l]_{B=0}\ , \tag{10}$$

and ρ_{ij} is the zero-magnetic-field resistivity. The coefficients of equations (9) and (10) are called the galvanomagnetic coefficients. They are linked to the conductivity coefficients by the reciprocal relation

$$\rho_{ij}(\vec{B})\sigma_{ij}(\vec{B}) = \delta_{ij} \tag{11}$$

Both ways of expressing the transport effects, as given by equations (1) and (11), are useful. When one assumes a particular model and band parameters for a solid, it is easier and more convienient to calculate the magnetoconductivity coefficients as opposed to the galvanomagnetic coefficients. When making experimental measurements on the materials, however, measurements of the galvanomagnetic coefficients are the least difficult of the two. This is

particularly true in semiconductors where problems with contacts are ever present. One method of making magneto-conductivity measurements is to use rectangular samples having a small length to width ratio with large area current contacts on the ends. The direction of the electric field $\vec{E}$ is then fixed and independent of $\vec{B}$. The problem, as mentioned above, is in making and ascertaining that the sample has uniform effective low resistance contacts. On the other hand, galvanomagnetic measurements require that the direction of the current density $\vec{J}$ be fixed and independent of $\vec{B}$. This is accomplished by using samples with large length to width ratio and current contacts at the ends. This type of measurement and configuration was chosen for this study.

The range of the indices of the coefficients is from one to three. The number of coefficients generated is then: $\sigma_{ij}(0) = 9$ each, $\sigma_{ijk} = 27$ each, $\sigma_{ijkl} = 81$ each, etc...; however, they are not all non zero nor independent. The number of non zero independent coefficients and relationships among them is determined by the application of Onsager's relationships and the symmetry requirements of the material. These requirements have been studied by several investigators of which Kao and Katz (17) is a good example. The source used in this study is found in the appendix of reference (16). There are two independent resistivity coefficients (ρ_{11}, ρ_{33}), two independent Hall coefficients (ρ_{132}, ρ_{213}), and six independent

magnetoresistivity coefficients (ρ_{1111}, ρ_{3333}, ρ_{1122}, ρ_{1133}, ρ_{3311}, ρ_{1331}).

In addition we find the following relations:

$$\rho_{22} = \rho_{11}, \quad \rho_{123} = -\rho_{213},$$

$$\rho_{231} = \rho_{312} = -\rho_{321} = -\rho_{132},$$

$$\rho_{1111} = \rho_{2222}, \quad \rho_{1122} = \rho_{2211}, \quad \rho_{1133} = \rho_{2233},$$

$$\rho_{3311} = \rho_{3322}, \quad \rho_{2323} = \rho_{3223} = \rho_{3131} = \rho_{1331},$$

$$\rho_{1212} = \rho_{2112} = \tfrac{1}{2}[\rho_{1111} - \rho_{1122}]. \tag{12}$$

The inversion relationships of equation (11) have also been worked out and are as follows:

$$\rho_{11} = \frac{1}{\sigma_{11}}, \quad \rho_{33} = \frac{1}{\sigma_{33}}, \quad \rho_{132} = -\frac{\sigma_{132}}{\sigma_{11}\sigma_{33}},$$

$$\rho_{213} = -\frac{\sigma_{213}}{\sigma_{11}^{2}}, \quad \rho_{1111} = -\frac{\sigma_{1111}}{\sigma_{11}^{2}},$$

$$\rho_{3333} = -\frac{\sigma_{3333}}{\sigma_{33}^{2}}, \quad \rho_{1122} = -\frac{\sigma_{1122}}{\sigma_{11}^{2}} - \frac{\sigma_{132}^{2}}{\sigma_{11}^{2}\sigma_{33}},$$

$$\rho_{1133} = -\frac{\sigma_{1133}}{\sigma_{11}^{2}} - \frac{\sigma_{213}^{2}}{\sigma_{11}^{3}}, \quad \rho_{3311} = -\frac{\sigma_{3311}}{\sigma_{33}^{2}} - \frac{\sigma_{132}^{2}}{\sigma_{11}^{2}\sigma_{33}},$$

$$\rho_{1331} = -\frac{\sigma_{1331}}{\sigma_{11}\sigma_{33}} + \tfrac{1}{2}\frac{\sigma_{132}\sigma_{213}}{\sigma_{11}^{2}\sigma_{33}}. \tag{13}$$

Knowing the independent coefficients and the relationships given by equation (12), one can write out equation (7) in detail and determine the minimum number of samples required to measure these coefficients. Only two types of

crystals are required; one with current parallel to the c-axis and one with current perpendicular to the c-axis. Figure 1 illustrates the orientations and probe placements chosen for this study. In part (a) the orientation of the cartesian coordinate system relative to the crystalographic axes is illustrated. Parts (b) and (c) then illustrate the sample orientations relative to the cartesian coordinate system. The resistivity and magnetoresistance are measured with probes 3 and 4. Hall effect potentials are measured by connecting a potentiometer between probes 3 and 4. With current flowing in the sample and zero magnetic field, the arm of the potentiometer is adjusted for zero potential between probes 5 and 6. The Hall potential then appears between probes 5 and 6 when a magnetic field is applied.

All of the coefficients can be measured by properly orientating the sample in the magnetic field with the probe placements as illustrated. In addition some redundant measurements may be taken. Additional redundant measurements could have been taken by placing another set of probes at right angles to the ones shown; however, it was felt that the disturbing influence of the additional probes would outweigh the advantage of redundant measurements.

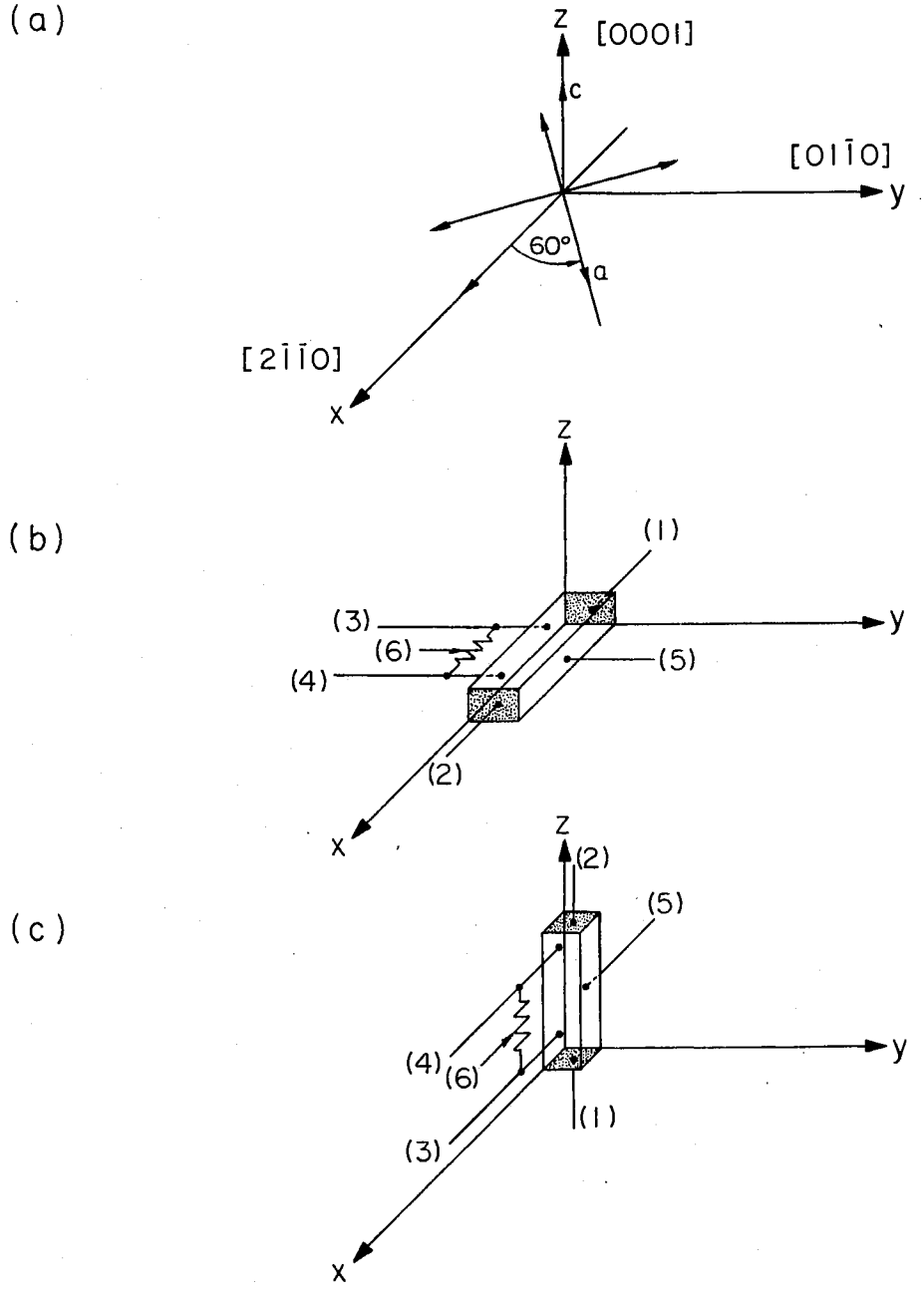

(a) Orientation of cartesian coordinate axes relative to the crystallographic axes, (b) Orientation and probe placement of type 1 samples, (c) Orientation and probe placement of type 2 samples.

Figure 1. Orientation of Samples.

CHAPTER II

EXPERIMENTAL PROCEDURE

Sample Preparation

The raw ZnO single crystals used in this study were purchased from the 3M Company and had less than 55 parts per million impurities as determined by emmission spectroscopy. The crystal boule had a hexagonal shape with dimensions of approximately 7mm diameter by 20mm long. The external features indicated that the long axis of the boule was the c crystalograph axis. This was confirmed with back reflection Laue x-ray photographs. The two end faces perpendicular to the c-axis were etched in a 30 percent solution of HNO_3. One of the surfaces exhibited etch pits. Following the suggestion of Watanabe et al. (18), this was designated as the (0001) surface thus defining the [0001] direction.

The boule was cut into rectangular pieces using a string saw. The cutting element of the saw consisted of a 0.01 inch diameter steel wire in the form of a continuous loop driven by a variable speed electric motor. The cutting surface was fed with a continuous stream of slurry containing number 600 grit aluminum oxide powder. A special

jig was constructed and the rectangular bars were hand lapped to the approximate final dimensions using number 600 carborundum waterproof paper. The samples were then polished to final dimensions using a slurry containing number 600 grit aluminum oxide. The sample orientations were checked and corrected at intermediate steps in the shaping process with the Laue back reflection x-ray equipment. From measurements made on the finished samples it is estimated that the sample axes deviate no more than two or three degrees from the associated crystalographic axes.

There are several factors to consider in determining the final dimensions of the sample. The maximum lengths of type 1 samples were 5 mm due to the dimensions of the available material. The bore of the electromagnet used was one-half inch. Since both longitudinal and transverse orientations of the sample are required this limits the maximum length of a sample to approximately 10 mm after allowing for mounting hardware. Measurement errors can arise due to sample geometry, contact size, and contact placement. A summary of the investigation of these effects appears on page 54 of Beer (3) and on page 317 of Weiss (19). It is shown that for a low mobility semiconductor such as ZnO negligible error will result provided that the length to width ratio is three or greater, the potential probes are spaced at least the width of the sample from the current end contacts, and the potential contacts are small relative to the width of the sample. The final dimensions of type

1 samples were approximately 1 x 1 x 5 mm^3 and type 2 samples were 1 x 1 x 9 mm^3.

Sample Contacts

In preparing samples the greatest amount of time was spent in learning how to make usable electrical contacts. Investigators who have studied ZnO make only brief mention of their techniques and methods of making electrical contacts. Harrison (10) nickel plated the ZnO surface and then soldered to the plating. Hutson (12) mentions that indium and gallium wet ZnO and used blobs of gallium at the sample ends for current contacts and indium coated phosphor bronze wires for potential probes. Hutson also mentions that the potential probes were improved by "forming" (discharging a small capacitor through the contact). In his conductivity measurements Thomas (20) used platinum wire loops around the sample and forming by capacitance discharge to make the electrical contacts. Aven and Swank (21) suggest the following guidelines in making ohmic contacts to wide-band-gap semiconductors: Employ a contacting material of high work function on p-type material and low work function on n-type material and create a region of high carrier concentration under the contact through either alloy regrowth or in-diffusion of a suitable dopant provided by the contacting material. ZnO is an n-type semiconductor with a work function of 4.68 electron volts and is commonly used as a dopant; therefore, indium satisfies

the general guidelines for a contacting material and was used in this study.

Current contacts applied to the ends of the sample were the first type attempted. It was found that the indium did wet and adhere to the ends forming reasonably good ohmic contacts after a little experimentation with soldering iron temperatures. There was a wide variation in contact resistance, however, from sample to sample and for repeated trials on the same sample. The following procedure evolved after much experimentation with surface preparation such as abrading, sand blasting, and etching with various types of etchants. The sample was etched for about two minutes in a ten percent solution of HCl, rinsed in distilled water, and dried. Soldering iron temperature was important. The temperature was adjusted by reducing the power input to approximately two thirds of that used for tin-lead soldering. All excess indium was wiped from the tip except for a small mirror-bright blob. Indium was applied to the ends of the sample using medium pressure and a scrubbing motion. One could feel and hear a sound similar to chalk on a slate board when the indium was wetting and adhering properly. Fine copper wire was then soldered to the ends and the resistance of the sample and the contacts were checked with an ohmmeter. The contacts were usually ohmic but much higher in resistance than that which was desired. The contact resistance was then lowered by what is believed to be a diffusion or doping process which occurred when a

heavy current was passed through it. Power dissipation in the contact and sample raised the temperature to approximately 600°C for a few seconds. The temperature was estimated on the basis of color. This heating procedure was repeated several times until no further decrease in contact resistance was observed.

The apparatus used for making potential contacts was a thermal compression bonding unit. The first successful contacts were made using 0.001 inch diameter gold wire. The wire was severed using a micro torch producing a gold ball approximately two or three thousands of an inch in diameter on the tip of the wire. The sample was then heated to approximately 450°C and the gold ball pressed onto the sample surface. This produced a good mechanical joint, but the contact resistance was generally quite high and non ohmic. The contact resistance was then reduced by a "forming" process by discharging a capacitor through the contact. It was observed that the polarity of the sample must be positive with respect to the potential lead in the forming process. A reversed polarity increased the contact resistance. Two or three samples were prepared using this type contact; however, a better method of making potential contacts was sought because the probability of making a good contact on the first trial was quite small. The "forming" process destroyed the contact more often than it improved it. The failure rate was not significantly reduced by variations in the energy of the discharge. A

technique was then developed for making indium potential contacts. A gold ball was formed on the wire as previously described. A hot soldering iron with a small mirror-bright blob of indium was touched to the gold ball and withdrawn. The excess indium was cut off with a stroke of a razor blade. This left a one to two thousands of an inch thick coating of indium on the bottom surface of the gold ball. The fresh indium surface was pressed onto the surface of the sample using the thermal compression bonding unit. The contact was heated enough to melt the indium by passing a heavy current through the contact for a few seconds The gold ball was compressed simultaneously with the pulse of current to create a good mechanical and electrical contact. Localized heating of the joint was necessary when making multiple contacts; otherwise, an elaborate jig would have been necessary to keep the previously soldered contacts from falling off while working on a new contact. Unless otherwise noted, all data were taken on samples with indium potential probes attached as described above.

Design of Sample Holder

The basic features of the sample mount are illustrated in Figure 2. The primary components are: (1) a half inch diameter phenolic rod with a transverse and longitudinal slot cut into it, (2) sub assembly mount, (3) coil mount. The whole assembly forms a snug fit in the bore of the electromagnet. The coil mount (3) consists of a ten turn

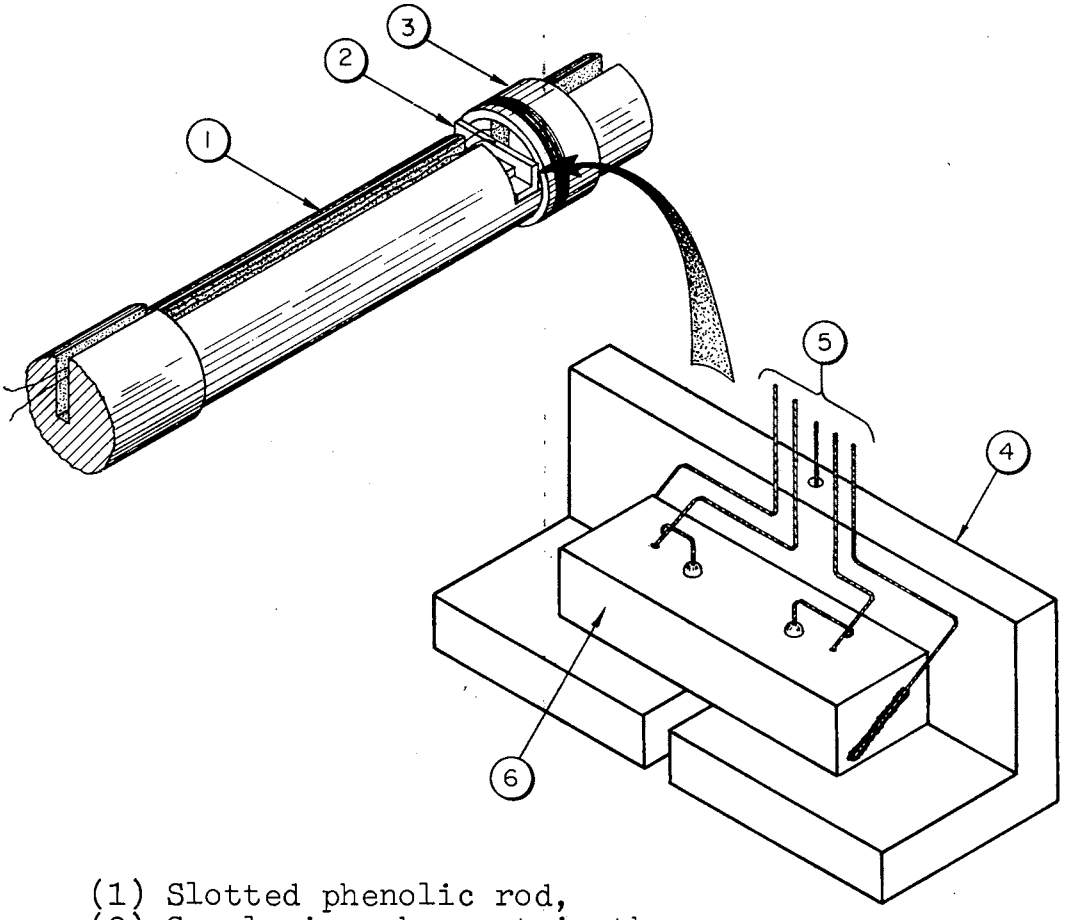

(1) Slotted phenolic rod,
(2) Sample in sub mount in the transverse measurement position, (3) search and bucking coil form, (4) Sample sub mount shown in greater detail, (5) Five insulated magnet wires twisted together to form the connecting cable, (6) Sample with details of potential probe placement.

Figure 2. Sample Holder and Mounting Details.

search coil which supplies an output proportional to the magnetic field strength and two bucking coils of one turn each. The bucking coils supply a potential to buck out undesired emfs induced on the signal leads of the sample.

Details of the sub-assembly mount (2) are shown in the inset of the figure. The basic part is an "L" shaped piece (4) which was machined out of a phenolic material. A twisted cable of five insulated #36 copper wires lead to the sub-assembly and are fanned out and epoxied to the inside lip of the phenolic sub-assembly. The ZnO sample (6) is cemented into the cradle of piece (4). Two gold potential leads are shown on the upper surface and are connected to the copper lead-in wires. The third potential lead (not shown in the illustration) is attached to the bottom surface of the sample.

The sub-assembly mount (2) fits snugly into either the transverse or longitudinal slots of the phenolic rod (1) and is cemented into place. As an additional feature the sub-assembly mount may be rotated 90 degrees so that the magnetic field is either perpendicular or parallel to the potential probe surface.

Measurements of angular magnetoresistance data and planar Hall effect data were taken using phenolic rods with the transverse slot cut at angles of 30°, 45°, and 60°.

Pulsed Magnet System

The magnetic fields used in this study were produced

by discharging a bank of capacitors into a wire-wound electromagnet. The capacitive energy storage system and controls were designed and built by personnel of this laboratory. A considerable amount of redesign and modification of the control circuitry was done by the author. K. J. Russell (22) and L. C. Laskowski (23) made high pulsed field magnetoresistance studies of semiconducting diamonds using this pulsed magnet system.

A simple schematic diagram of the system is illustrated in Figure 3. The basic elements of the pulsed magnet system are a capacitor, a switch, and an electromagnet. These, along with the internal resistance of the electromagnet and connecting leads, form a simple L-C-R circuit. When the capacitor is discharged through this electromagnet the magnet current waveform is the familiar damped sinusoidal shape. The magnetic field waveform is a like function of time since it is proportional to the current.

Only the first half cycle of current flow is needed for the purpose of taking data in a magnetic field. The unused energy will be dissipated over a period of several cycles in the resistance of the electromagnet if the oscillating current is allowed to continue. This heats up the electromagnet and places extra stress on it as well as on the capacitors thus shortening the life of both. The function of the crowbar circuit is to dump the energy remaining after one half cycle into a dummy load and thus extend the life of the magnet and capacitors.

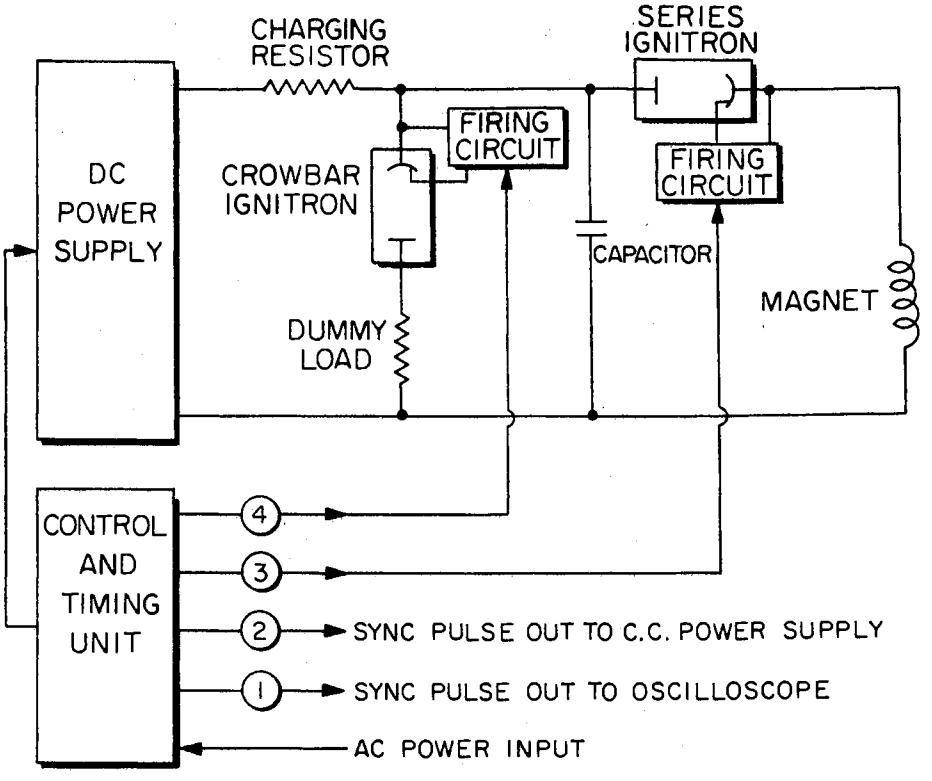

Figure 3. Simplified Schematic of the Pulsed Magnet System.

The capacitor bank actually consists of fourteen 180 microfarad capacitors connected in parallel. They can be charged to 6,000 volts and have an energy storage capability of approximately 45 kilojoules. The series ignitron shown is actually 14 units in parallel and the crowbar ignitron consists of 8 units in parallel.

Other features included in the system are manual or automatic operation of the charging and discharging cycle and many safety features for the protection of the equipment and operating personnel.

Electromagnet

The high magnetic fields were produced by a mulitlayer copper coil electromagnet. The design of this type electromagnet, as well as many other types, is given in a review written by D. B. Montgomery (24). A cross section of the magnet is shown in Figure 4, and Table I lists the parameters and performance of the completed magnet. The construction details are as follows. A special winding jig was constructed to hold the 200 pound roll of magnet wire and the magnet spool (a) which was machined out of a linen based phenolic. A total of 273 turns of AWG size 10 square cross section insulated magnetic wire (b) was wound onto the spool in 10 layers with fiberglass cloth between each layer. Heavy tension was maintained on the wire during the winding process. The insulating spool with wire was slipped inside of a pre-wound 0.57 cm wall epoxy-fiberglass

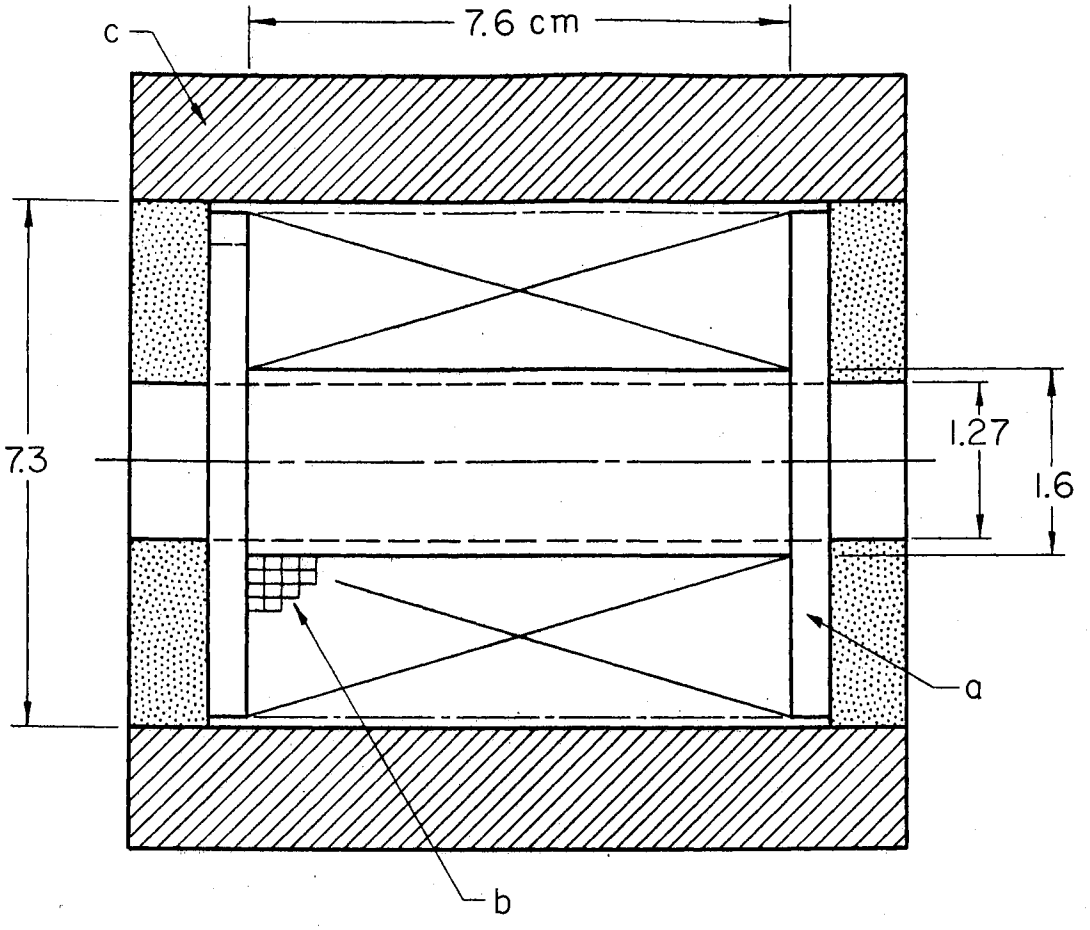

(a) Phenolic spool, (b) Square cross section insulated magnet wire wound on spool, (c) Fiberglass retaining sleeve.

Figure 4. Construction Details of Wirewound Electromagnet.

TABLE I

PARAMETERS AND PERFORMANCE OF THE WIREWOUND ELECTROMAGNET

Inside Diameter of Coil	1.6 cm.
Outside Diameter of Coil	7.3 cm.
Length of Coil	7.6 cm.
Diameter of Magnet Bore	1.27 cm.
Total Number of Turns of Wire	273
Number of Layers of Wire	10
Wire Type	Essex Wire Corp. Heavy Allex Film Insulation, AWG Size 10, Square Cross Section
Thickness of Fiberglass Insulation between Layers	0.04 cm.
D.C. Resistance of Coil	0.14 ohms
Inductance of Coil	0.97 milli-henries
Half Period of Magnet	5 milli-seconds
Uniformity of Magnetic Field	0.6% for $\pm$ 0.6 cm. along axis
Peak Magnetic Field Produced	220 Kilogauss at 20 Kilojoules energy input

retaining sleeve (c) and sealed in place with epoxy. The sealed unit was then connected to a vacuum system for 24 hours to de-gass the unit. Two vacuum ports, one on each end of the spool, had been included in the design of the spool. During this time the unit was heated to approximately 100°C by means of a heavy AC current through the coil to aid the de-gassing process. It was then vacuum impregnated with epoxy and placed in an oven to cure.

Additional reinforcement was provided by a one inch thick linen filled phenolic plate (not shown in the figure). A hole was cut in the plate. The plate was slipped over the sleeve (c) and epoxied in place around the middle of the coil. Two threaded bolt holes in the plate allowed the unit to be bolted to the output terminals of the pulsed magnet system. The magnet coil was connected to the terminals by means of flexible leads. The direction of the magnetic field was reversed when taking data by reversing the flexible leads.

Electronic Measurement Apparatus

There are several difficulties encountered in making galvanomagnetic measurements on ZnO in a pulsed magnetic field. The three major problems are: The short duration of the data pulse, an induced electromotive force (emf) in the signal leads, and the fact that magnetoresistance effect is very small in ZnO. The approach taken is essentially an extension of the DC techniques used at low fields. It is

similar in many respects to the methods used by Kapitza (25), who was the first to study magnetoresistance effects using pulsed fields. The basic measurement technique is as follows: send a pulse of current through the sample; during the current pulse trigger on the magnetic field pulse to the sample; finally, observe the change in potential on the signal leads due to the application of the magnetic field pulse to the sample. The DC current of sufficient magnitude to observe the magnetoresistance effect would heat up the sample excessively; therefore, a pulse of current must be used. Additional advantages of a current pulse is that it eliminates troublesome thermal emfs and interferring thermomagnetic effects. The pulse duration is less than 10 milliseconds which is too short for thermal emfs to develop. The temperature of the sample also remains relatively constant during the measurement period.

The measuring circuit shown in Figure 5 has been simplified as an aid in understanding the method of signal measurement. Only the simplified details for making magnetoresistance measurements are shown. Not shown in the drawing are such details as switches for reversing the sample current, switches for selecting the magnetoresistance potential probes or the Hall potential probes, contact and connections for the Hall potential measurement.

The detection and recording of data was done with a Type 551 Tektronix dual-beam oscilloscope and a Hewlett Packard Model 196 A oscilloscope camera. Type "D" and "O"

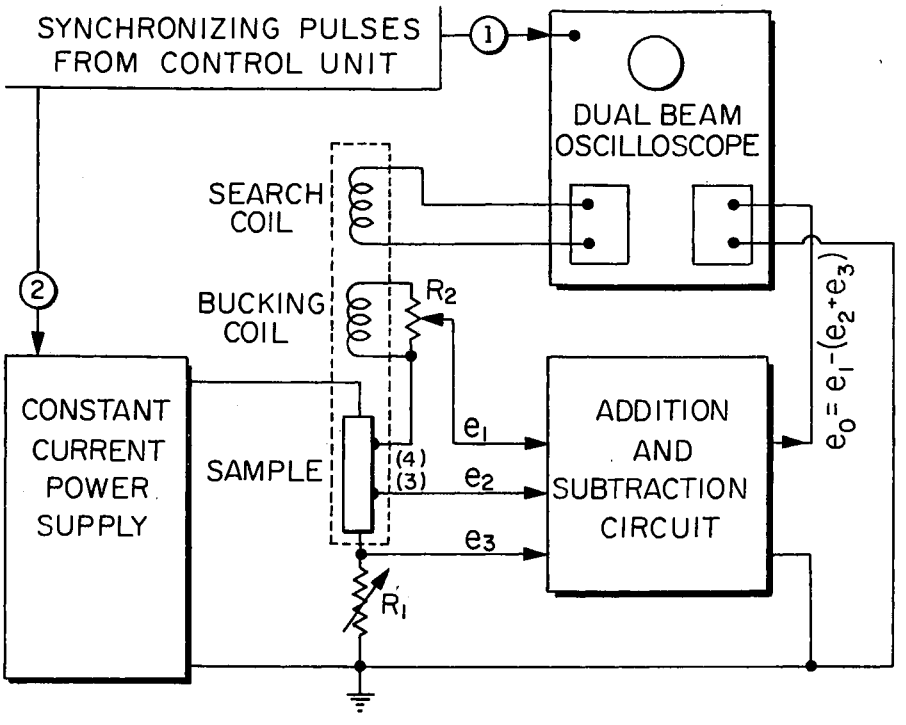

Components enclosed in dotted lines are located in the bore of the magnet.

Figure 5. Simplified Schematic of the Magnetoresistance Measuring Circuit.

preamplifiers were used with the scope. A potential proportional to magnetic field strength was displayed on one trace of the scope and the measured data was displayed on the other trace.

The magnetic field in the electromagnet was measured with a search coil connected to one input of the oscilloscope through an R.C. integrator. One of the operational amplifier channels of the Type "O" oscilloscope plug-in was connected as an integrator and used in this measurement of magnetic field. The search coil consisted of ten turns of fine wire wound on a coil form and located relative to the sample as shown in Figure 2. The magnetic field at any instant of time was obtained by multiplying the height of the oscilloscope trace by a constant. The constant was determined by knowing the area-turns of the coil, the integrator time constant, and the oscilloscope sensitivity setting. The same coil was used in all measurements.

As mentioned previously, a heavy pulse of current was used in making measurements. The constant current power supply was constructed using a variable constant voltage power supply, a General Radio Type 1217-C Unit Pulse Generator, and a transistorized circuit designed by the author. The transistorized circuit is a gated variable impedance connected in series with the load composed of the sample and resistor, R_1. It effectively converts the constant voltage power supply to a constant current power supply. The Unit Pulse Generator supplies a gating pulse to

the transistor circuit that is synchronized with the oscilloscope sweep and the discharge of the capacitor bank into the electromagnet. A current of approximately 70 milliampers flows through the sample only during the gate "ON" period of approximately 8 milliseconds. The magnitude of the sample current is determined by measuring the pulse voltage across a calibrated resistor which forms a part of resistor R_1. The magnetoresistance effect is characterized by the ratio $[V(B) - V(0)]/V(0)$, where V(0) is the difference in potential between probes three and four and V(B) is the potential difference in the presence of a magnetic field B. For ZnO, this ratio is approximately 10^{-4} when making transverse magnetoresistance measurements in a magnetic field of 20 kilogauss. If DC constant current could have been used, then $\delta V = V(B) - V(0)$ could be measured by letting $R_1 = 0$, and feeding the two probe outputs to the Type D preamplifier operated in the differential amplifier mode with AC coupling. With a pulsed constant current supply, however, both δV and V(0) appeared on the signal trace of the oscilloscope using this method of measurement and δV could not be detected in the presence of V(0). V(0) had to be eliminated from the signal channel before δV could be measured.

Figure 5 illustrates the method used to subtract out V(0) from the signal channel. The second operational amplifier channel in the Type O plug-in unit was set up to function as an addition and subtraction circuit. With the

magnetic field equal to zero a series of current pulses were sent through the sample and R_1. R_1 was then adjusted so that $e_o = 0$ as observed on the oscilloscope. For this case, $e_1 - e_2 = e_3$. Now when the magnetic field was pulsed on during the current pulse, the resistance of the sample increased so that $e_1 - e_2 > e_3$. Since the current and R_1 were constant the value of $e_o = \delta V$ observed on the oscilloscope is a measure of the change in resistance of the sample.

The stability requirements for the constant current power supply during the current pulse are easier to achieve since e_3 is a function of sample current. For example, if e_3 were produced in some other manner, such as a battery or variable voltage supply, it can be shown that $\delta V/V \simeq (\delta R)/R + (\delta I)/I$, where R is the resistance of the sample and δR is the change in resistance of the sample produced by the magnetic field. Now, since it is desired to measure the values of $\delta R/R$ as low as 10^{-4}, this requires that $\delta I/I \simeq 10^{-6}$ to obtain a reasonably accurate measurement of $\delta V/V$. This requirement for $\delta I/I$ is very difficult to meet. For the circuit illustrated, however, it can be shown that $\delta V/V \simeq (I + \delta I)(\delta R)/IR$. For this case $\delta I/I \simeq 10^{-2}$ will yield the same accuracy as the case illustrated above. Current stability of this magnitude and better is easily achieved.

As mentioned previously, one of the problems encountered when using pulsed magnetic fields is the generation

of an induced emf on the signal leads due to the changing magnetic field. All leads to the sample were tightly twisted together to reduce the area of the probe circuit; however, the pickup was still an order of magnitude greater than the magnetoresistance voltage change. A bucking coil was used to reduce the pickup to an insignificant level. It is a single turn coil wound on the same coil form as the search coil and located near or surrounding the sample in the bore of the magnet. The output of the bucking coil is connected in series with one of the signal probes and its phase and amplitude are adjusted so that its output is equal in amplitude but opposite in phase to the induced emf on the signal lead. Any remaining signal can be distinguished from the galvanomagnetic effects by its non-dependence on sample current.

CHAPTER III

MEASUREMENTS AND RESULTS

Measurement Techniques

If one could make measurements on a perfectly homogeneous sample with ideal gometry and contact placement, then only one measurement at a given field strength would be needed to determine the magnitude of the galvanomagnetic coefficient. This ideal is never achieved in practice, therefore, each measurement is a mixture of galvanomagnetic effects plus other interfering effects. To further separate these effects, the low field technique of taking measurements with both forward and reversed current and forward and reversed magnetic field was used. Each measured potential is assumed to be the sum of four potentials defined as follows:

δV_{EIEB} = Potential which is even with a reversal of current and even with a reversal of magnetic field,

δV_{EIOB} = Potential which is even with a reversal of current but odd with reversal of magnetic field,

δV_{OIEB} = Potential which is odd with a reversal of current but even with a reversal of magnetic field,

δV_{OIOB} = Potential which is odd with a reversal of both current and magnetic field.

The potential δV_{OIEB} was taken as a measure of the magnetoresistance effect and is given by the average of four

measurements

$$\delta V_{OIEB} = \tfrac{1}{4}[(\delta V_{I,B} + \delta V_{I,-B}) - (\delta V_{-I,B} + \delta V_{-I,-B})], \qquad (14)$$

where the subscripts have their obvious meaning regarding the direction of current and magnetic field. Likewise, the Hall effect was determined from the average

$$\delta V_{OIOB} = \tfrac{1}{4}[(\delta V_{I,B} + \delta V_{-I,-B}) - (SV_{-I,B} + SV_{I,-B})]. \qquad (15)$$

A few measurements were made on all the samples using all four combinations of current and magnetic field directions, but it turned out that only two measurements were necessary to separate the effects. The average potential for magnetoresistance was

$$\delta V_{OIEB} = \tfrac{1}{2}(\delta V_{I,B} + \delta V_{I,-B}), \qquad (16)$$

and for Hall effect

$$\delta V_{OIOB} = \tfrac{1}{2}(\delta V_{I,B} + \delta V_{-I,-B}). \qquad (17)$$

The following experimental routine was adopted for making magnetoresistance measurements. The sample was orientated as required to make measurements for the desired coefficient. With zero magnetic field, a series of data traces were observed on the oscilloscope as pulses of current were applied to the sample. Referring to Figure 5, R_1 was adjusted so that e_o was approximately zero. With zero sample current, the capacitor bank was discharged several times while observing the data trace on the oscilloscope. The amplitude and phase of the bucking emf were then adjusted so that the total induced emf was approximately zero. A calibration table of bank voltage vs. peak

magnetic field produced by a discharge was constructed. The bank was then charged up to the desired voltage. The oscilloscope camera lens was held open and the bank discharged. Two sets of data traces were on the same photograph, one trace for forward current and forward magnetic field and one trace with forward current and reversed magnetic field. The oscilloscope graticule was also recorded on the same photograph as a scale reference.

Figure 6 (a) is a line drawing of a data photograph. The upper pair of traces is the magnetoresistance probe output as a function of time and the lower pair of traces is a potential proportional to magnetic field as a function of time. The magnetic field trace labeled "+B" is associated with the probe signal trace labeled "$\delta V_{I,B}$", and the magnetic field trace labeled "-B" is associated with the probe signal trace labeled "$\delta V_{I,\ -B}$". Figure 6 (b) illustrates the relative timing of the output trigger pulses from the Control and Timing Unit shown in Figure 3. The dotted lines show the correlation of the occurrence of each pulse and the data traces of part (a). Pulse number one triggers the oscilloscope at time t_1, and the horizontal traces are begun. The constant current power supply is gated "ON" at time t_2. This causes a small vertical deflection to occur on the probe signal trace and defines a reference potential for the case of zero magnetic field. At time t_3, the series ignitrons in the capacitor bank are fired, and the capacitors begin to discharge through the

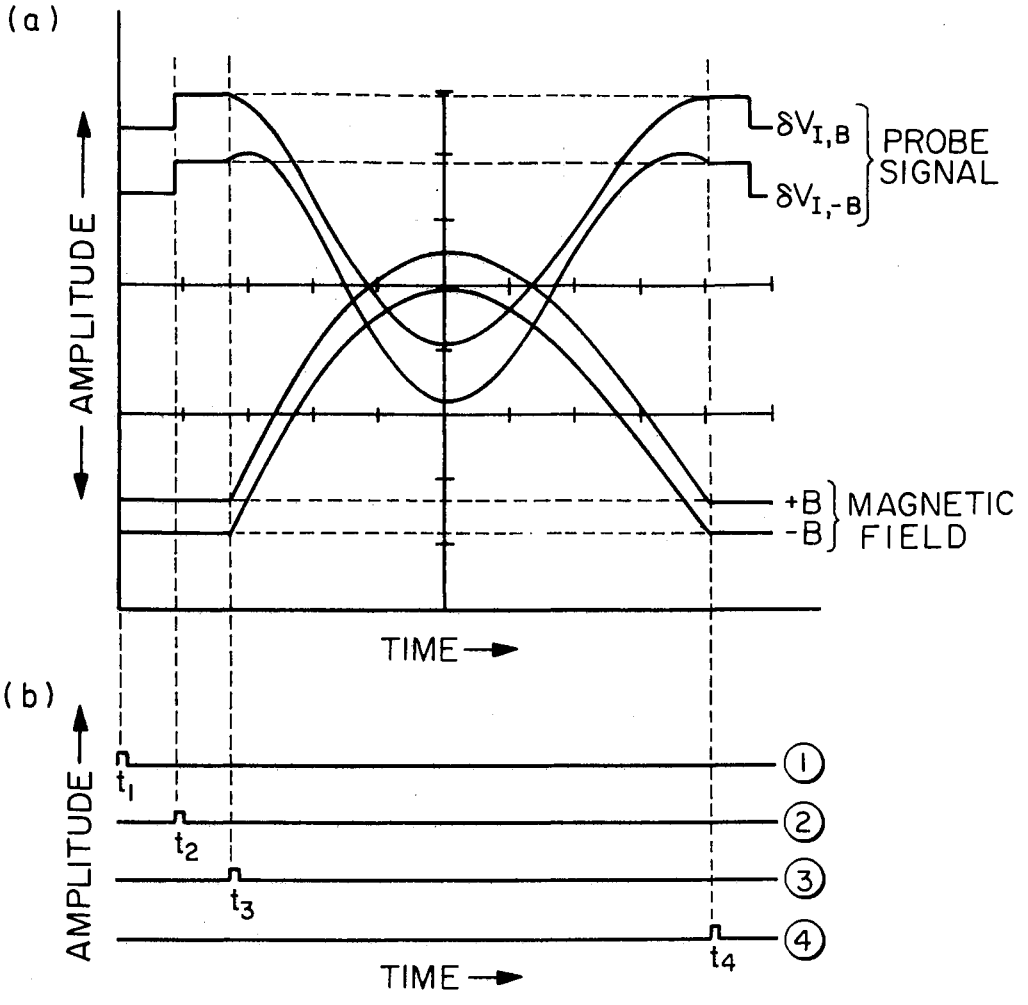

(a) Line drawing of oscilloscope photographic data. (b) Relative timing of the system timing pulses. The occurrance of the trigger pulses is correlated with the observed waveforms of the data traces. The trace number refers to the corresponding trigger pulse output from the Control and Timing Unit.

Figure 6. Illustration of Typical Magneto-resistance Data.

electromagnet. This point in time is quite evident on the data traces; the potential begins to increase on both the probe signal trace and the magnetic field trace. It is observed that the probe signal output is a maximum at maximum magnetic field. As evidenced by the magnetic field trace, the magnet current begins to fall after reaching a maximum, and at time t_4 it is zero. At this point, the crowbar ignitrons are fired, and the electromagnet is effectively disconnected from the capacitor bank. A short time after t_4 the gate pulse to the constant current power supply ends and the sample current drops to zero. This is evident on the probe signal trace as the potential drops back to the level at which the trace was begun. The horizontal dotted lines in Figure 6 (a) are the reference points for measuring the quantity $\delta V(B)$. A ruler is used to draw these lines on the photograph after it has been removed from the camera and processed.

Another feature illustrated in Figure 6 (a) is the difference in the waveform of the probe potential $\delta V_{I,B}$ as compared to the waveform given by $\delta V_{I,-B}$. This is due to the presence of a potential δV_{OIOB} mixed with predominant potential δV_{OIEB}.

It might be expected that a pair of data traces, both forward and reversed magnetic field, at a peak field of 200 kilogauss would be sufficient to evaluate any one of the coefficients over a large range of field values below the maximum. However the accuracy of the measurement was not

satisfactory for values less than approximately one-half of the peak field. The field range of 20 to 200 kilogauss was therefore covered using four to six sets of discharges. To further increase the accuracy of the measurements, the vertical sensitivity of the oscilloscope was adjusted and calibrated such that the peak deflection on each trace was in the range of three to four centimeters, four centimeters being the maximum allowed for each trace.

The relation used to calculate the resistivity of the samples is given by

$$\rho_{ij}(0) = E_i/J_j = V_i A/I_j l, \tag{18}$$

where V_i is the potential measured between probes 3 and 4 of Figure 1, l is the distance between the probes, A is the cross sectional area of the sample, and I_j is the current in the direction, j. The dimensions of the sample were measured with a traveling microscope. The distance, l, was the least accurate of these quantities since the point at which electrical contact was made was not necessarily coincident with the mechanical center of the contact. It is, however, estimated that the resistivity is accurate to within 8 percent based on data taken on different sets of contacts in a study of the homogeneity of the samples.

The samples were checked for evidence of mechanical imperfections and impurity gradients along the current directions. The number of usable samples on which measurements were made were; three each of type 1 (current along the a-axis), and one each of type 2 (current along the

c-axis).

Knowing the possible galvanomagnetic coefficients one can see how to evaluate these coefficients by substituting equation 8 into 7 and writing it out in terms of the possible non-zero coefficients. The equations for each orientation type sample are:

Type 1 Sample

$$E_1 = (\rho_{11} + \rho_{1111} B_1^2 + \rho_{1133} B_3^2)J_1 , \quad (19)$$

$$E_2 = (\rho_{213} B_3 + \rho_{2112} B_1 B_2)J_1 , \quad (20)$$

Type 2 Sample

$$E_1 = (\rho_{132} B_2 + \rho_{1331} B_3 B_1)J_3, \quad (21)$$

$$E_3 = (\rho_{33} + \rho_{3311} B_1^2 + \rho_{3322} B_2^2 + \rho_{3333} B_3^2)J_3 , \quad (22)$$

where subscripts 1, 2, and 3 refer to the x, y, and z axes respectively. These four equations include all possible coefficients to second order and each of the coefficients can be determined independently by properly orientating the sample relative to the magnetic field.

For purposes of analysis and comparison with the predictions of a theoretical model the first and second order galvanomagnetic coefficients are divided by the resistivity. These quantities are then independent of the number of carriers and can be compared from sample to sample. Solving for these ratios in terms of laboratory units of volts, amperes, gauss, gm., cm., and sec. yields the general relations,

$$\rho_{\alpha\beta\gamma} / \rho_{\beta\beta} = \frac{10^8}{B} \left(\frac{1}{w}\right)\left(\frac{\delta V}{V}\right) = \mu_H \qquad (23)$$

$$\frac{\rho_{\alpha\alpha\beta\beta}}{\rho_{\alpha\alpha}} = \frac{10^{16}}{B^2} \frac{\delta V}{V} \qquad (24)$$

where l is the distance between probes 3 and 4 and w is the width of the sample. The ratios given by equation 23 are the the Hall mobilities μ_H and those given by equation 24 are called the magnetoresistance coefficients.

Galvanomagnetic Coefficients

The results of the galvanomagnetic measurements made on two of the samples are shown in Figures 7 through 14. Each coefficient was measured as a function of magnetic field strength in the range of 20 to 200 kilogauss. This range was covered with four to six overlapping sets of data. Some of the data points shown are average values of several sets of photographic data. Plotted against magnetic field are: transverse magnetoresistance in Figures 7 through 10, longitudinal magnetoresistance in Figures 11 and 12, and Hall potential in Figures 13 and 14. The magnetoresistance voltage changes followed a simple B^2 magnetic field dependence to within $\pm$ 5 percent. No systematic deviation was observed. The Hall potential changes followed a simple B magnetic field dependence.

The measurement of the ρ_{1331} coefficient was the last to be attempted. During the mounting process, the crystal was fractured, therefore, this one coefficient was not

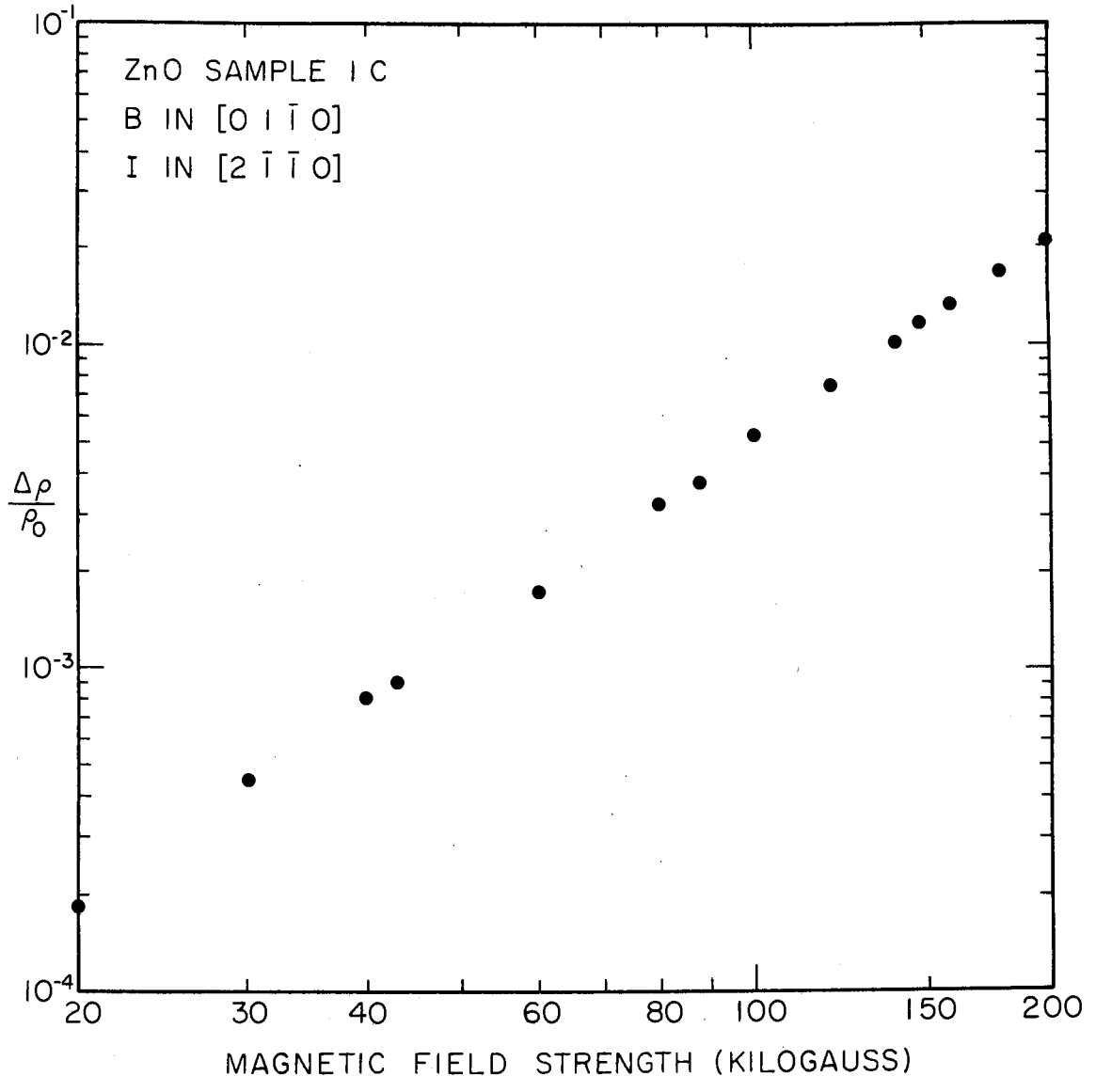

Figure 7. Variation of transverse magnetoresistance with magnetic field strength in ZnO sample 1C. Data used to calculate the magnetoresistance coefficient ρ_{1122}/ρ_{11}.

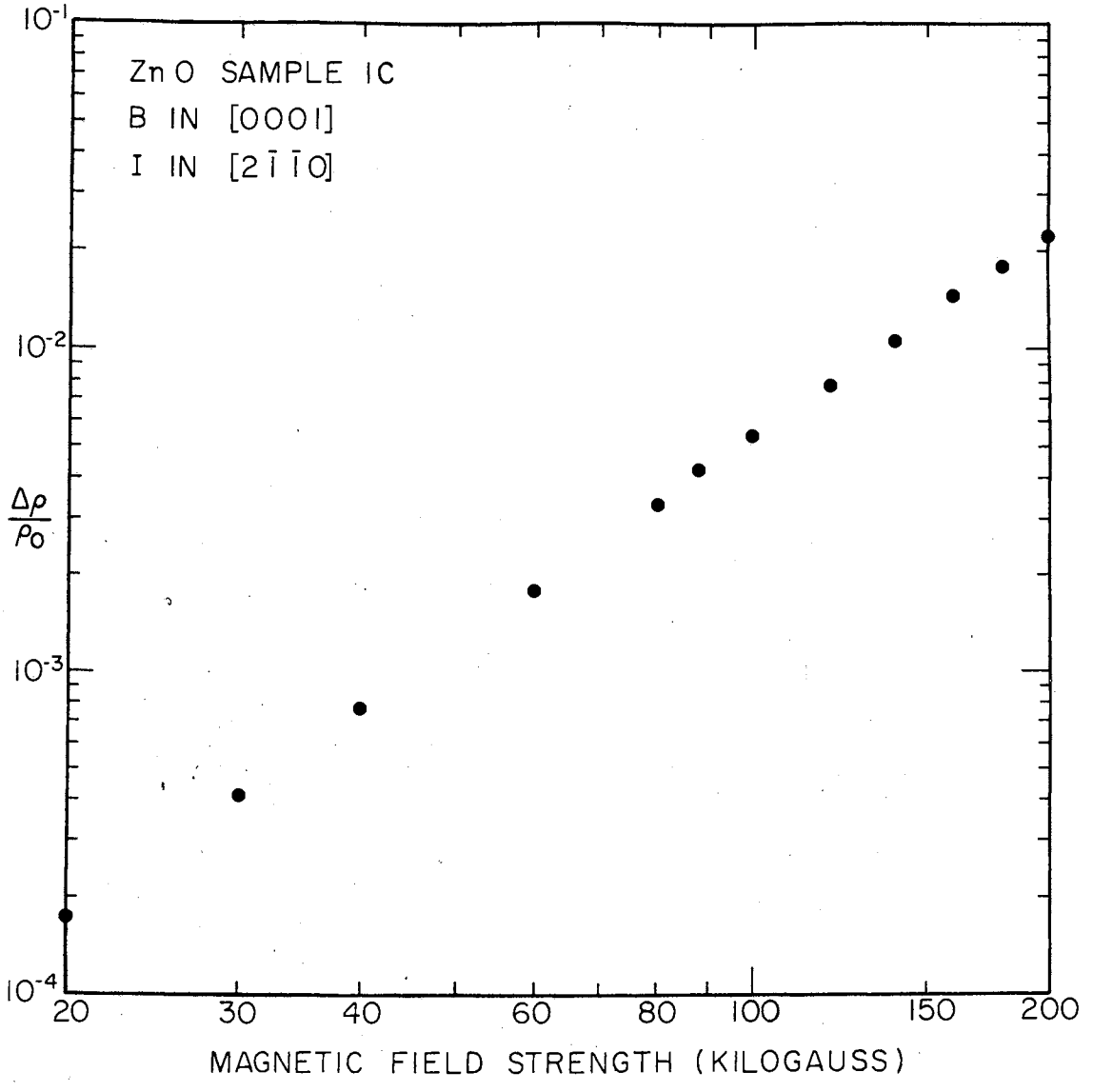

Figure 8. Variation of transverse magnetoresistance with magnetic field strength in ZnO sample 1C. Data used to calculate the magnetoresistance coefficient ρ_{1133}/ρ_{11}.

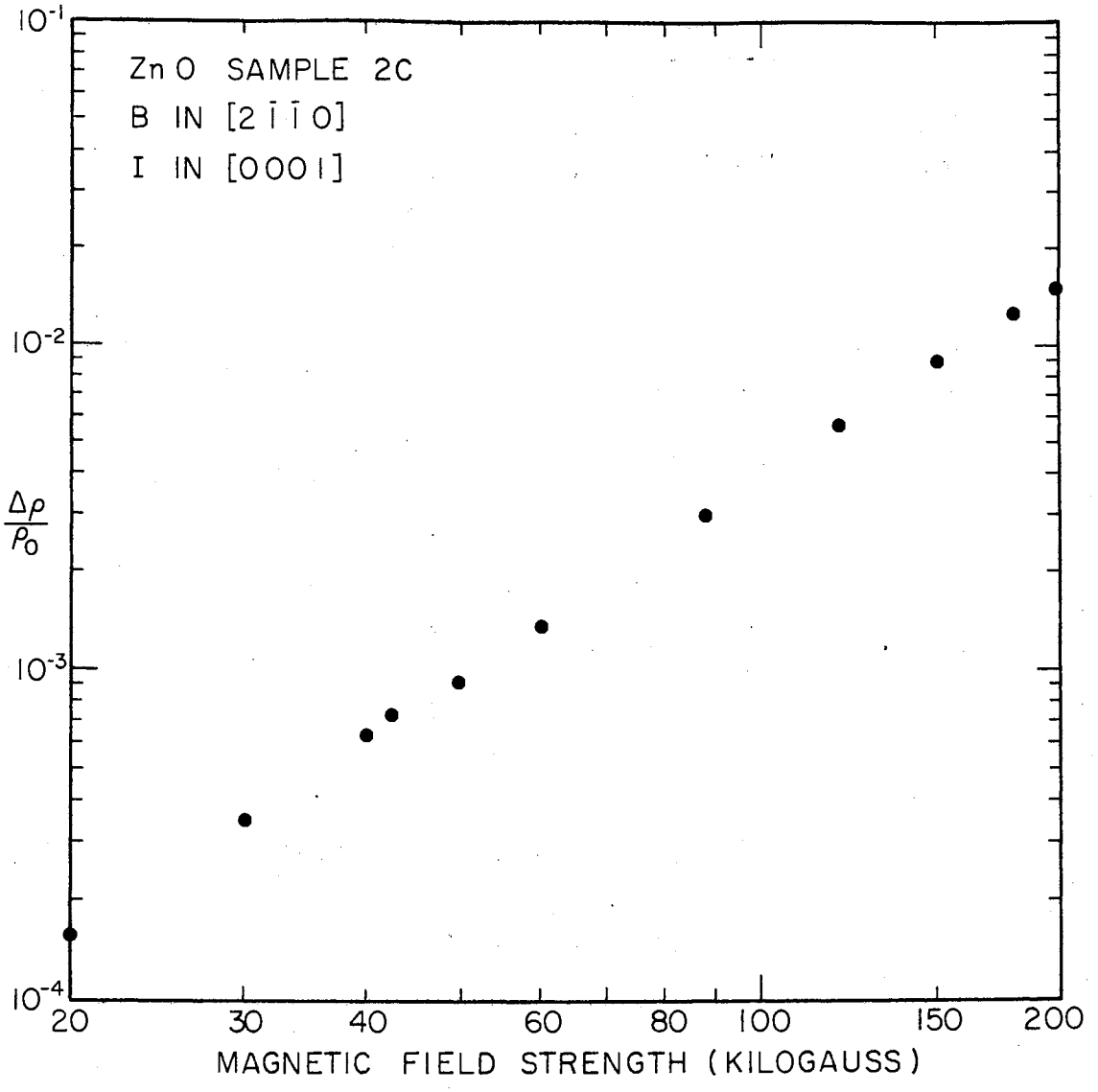

Figure 9. Variation of transverse magnetoresistance with magnetic field strength in ZnO sample 2C. Data used to calculate the magnetoresistance coefficient ρ_{3311}/ρ_{33}.

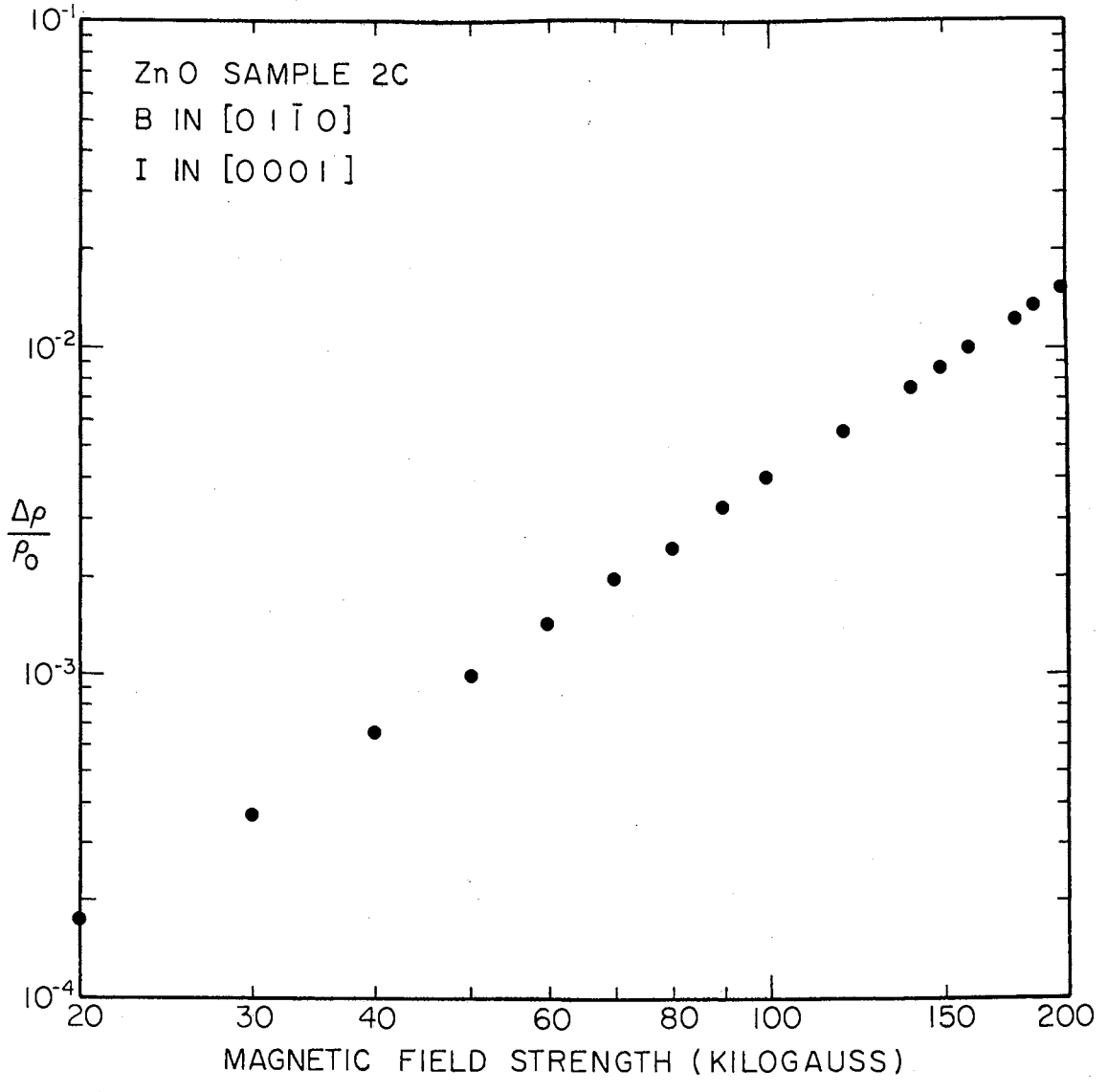

Figure 10. Variation of transverse magnetoresistance with magnetic field strength in ZnO sample 2C. Data used to calculate the magnetoresistance coefficient ρ_{3322}/ρ_{33}.

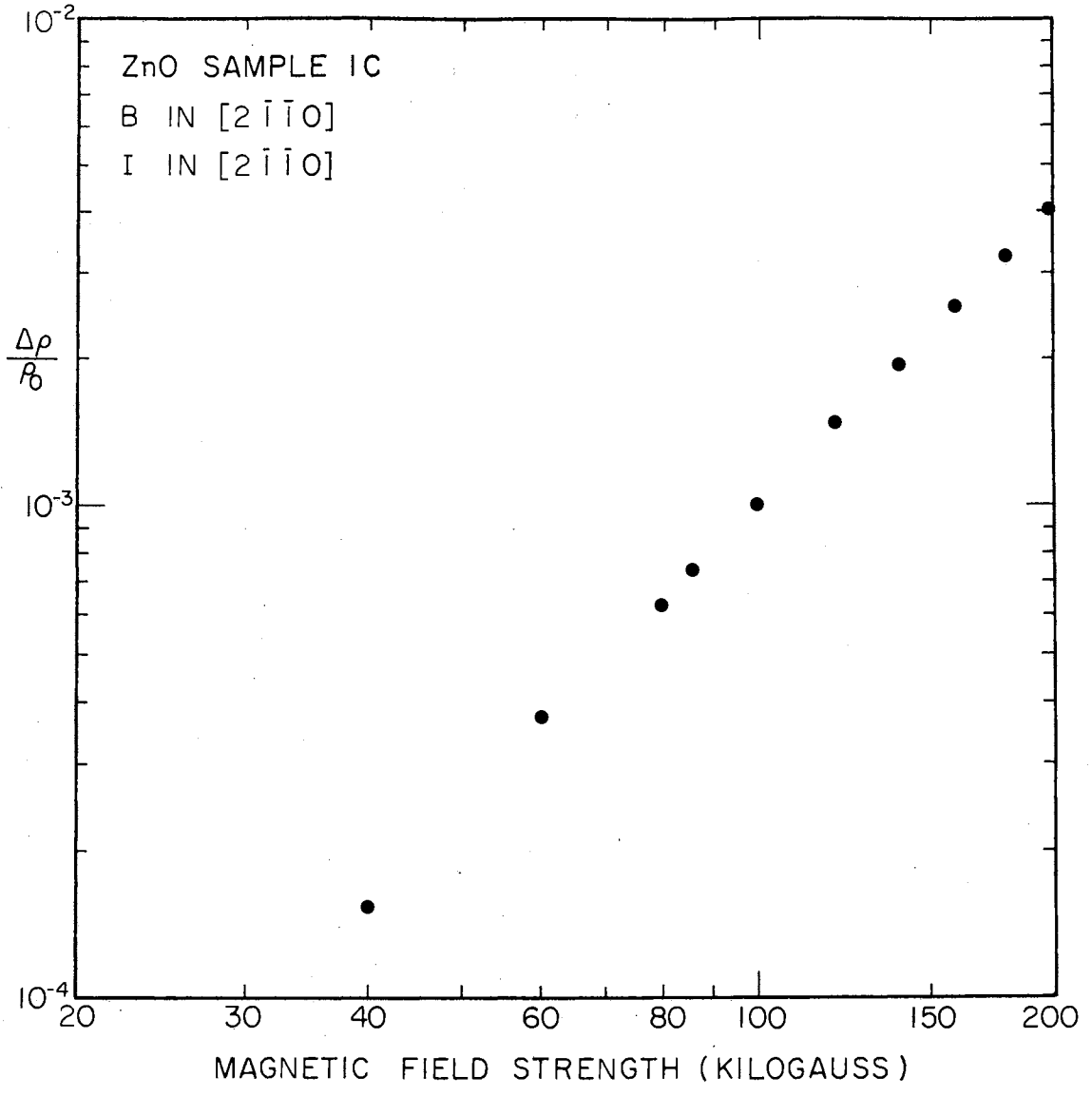

Figure 11. Variation of longitudinal magnetoresistance with magnetic field strength in ZnO sample 1C. Data used to calculate the magnetoresistance coefficient ρ_{1111}/ρ_{11}.

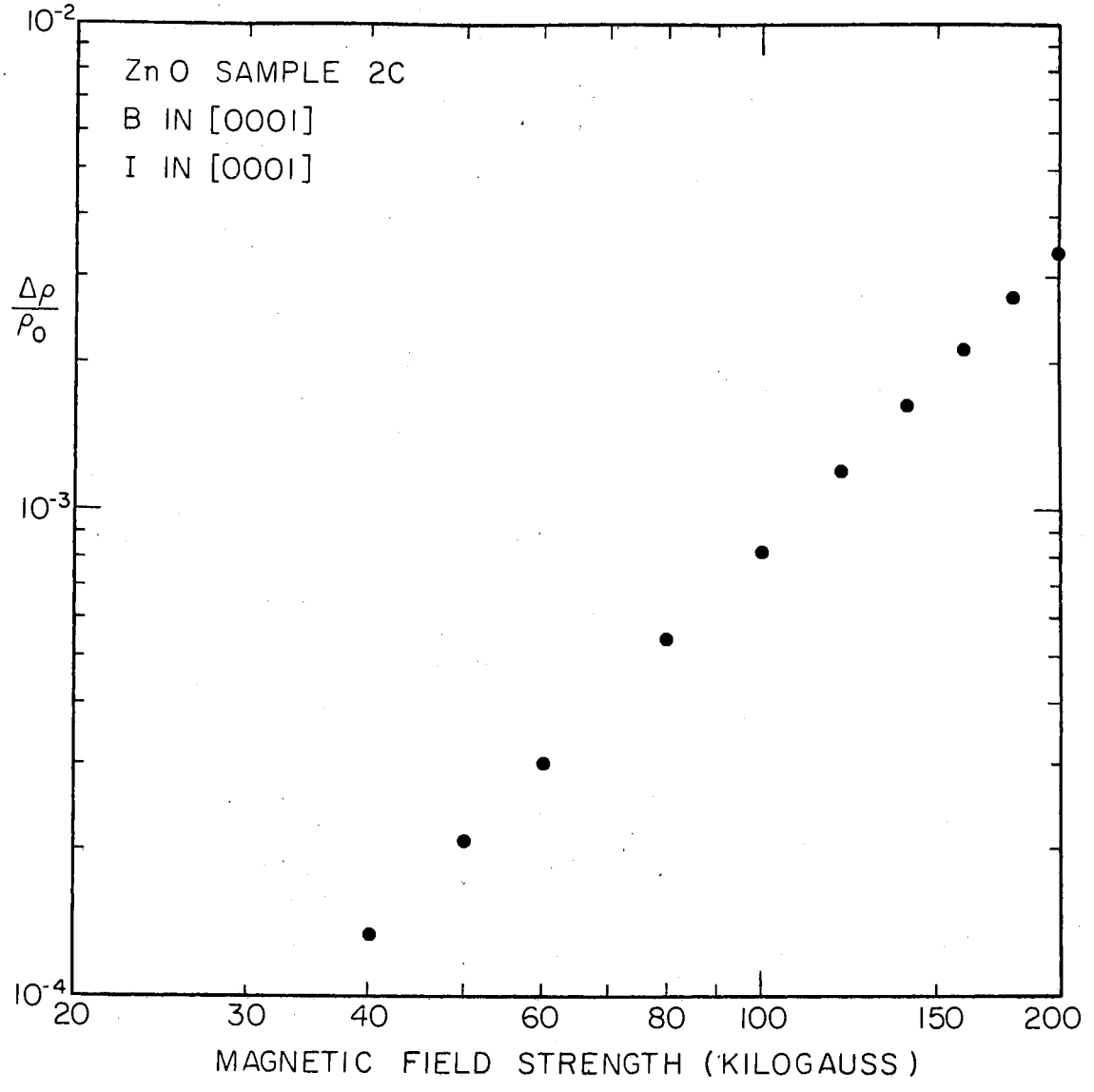

Figure 12. Variation of longitudinal magnetoresistance with magnetic field strength in ZnO sample 2C. Data used to calculate the magnetoresistance coefficient ρ_{3333}/ρ_{33}.

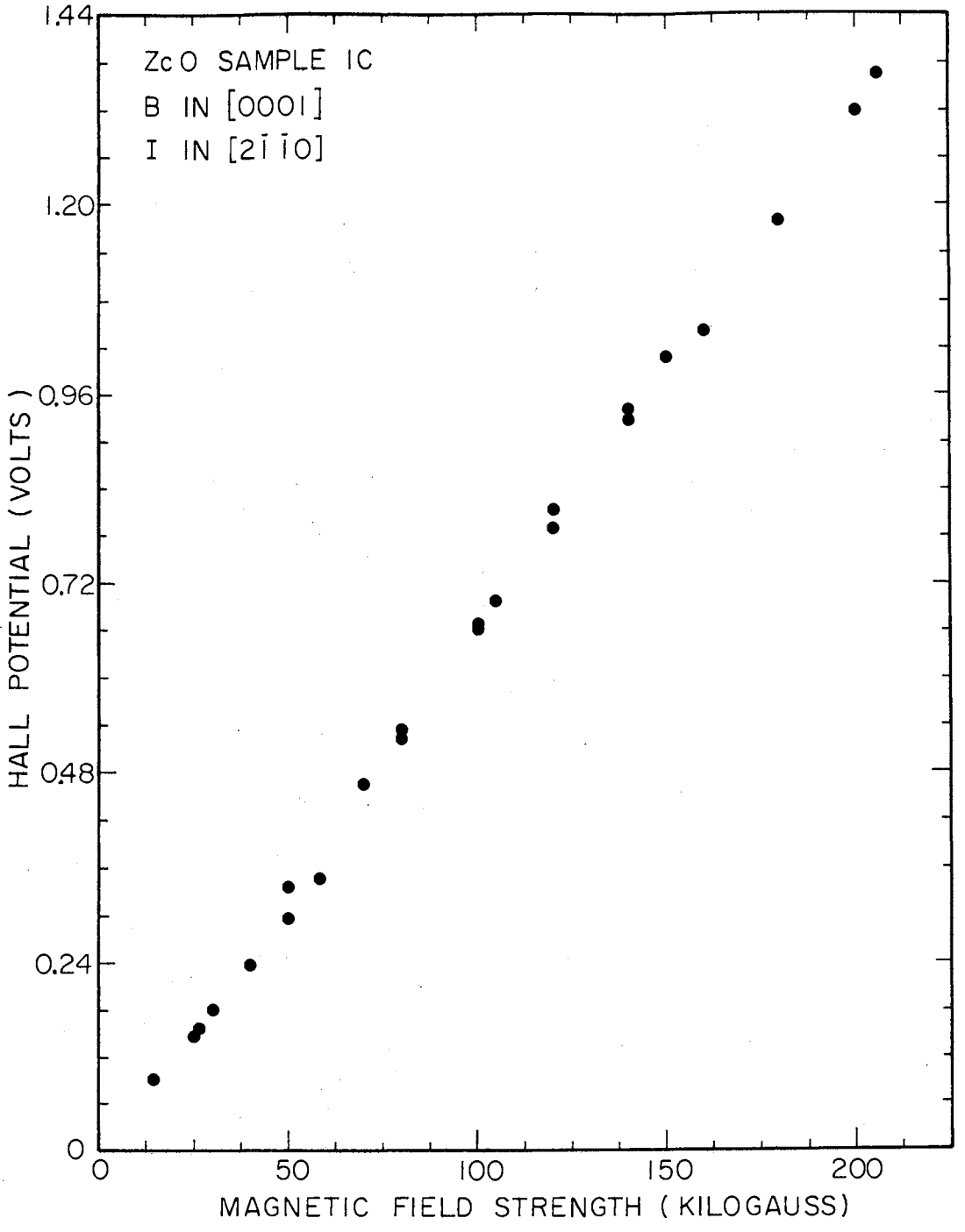

Figure 13. Variation of the Hall potential with magnetic field strength in ZnO sample 1C.

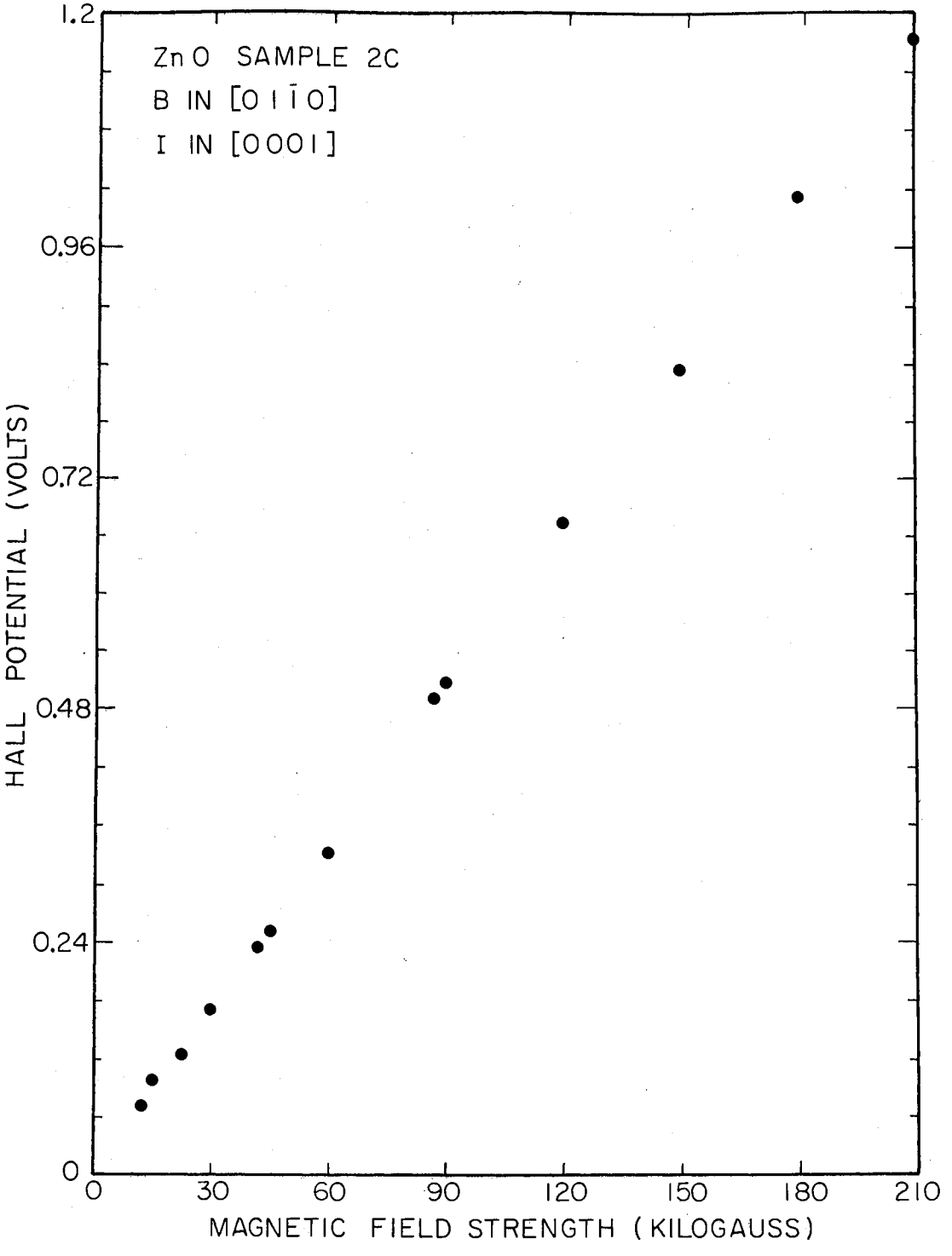

Figure 14. Variation of the Hall potential with magnetic field strength in ZnO sample 2C.

measured in this study.

The results of the measurements on all four samples are shown in Table II. The galvanomagnetic coefficients are defined by equations 9 and 10 as partial derivatives which are evaluated in the limit of zero magnetic field. The values of the magnetoresistance coefficients given by equation 24 were obtained by obtaining a "best fit" of the data to the relation

$$\frac{\Delta\rho}{\rho_o B^2} = b + aB^2 \qquad (25)$$

where a and b are constants and B is the magnetic field. The constant b then is equal to the magnetoresistance coefficient in the limit of zero magnetic field. The data was fed into an IBM Model 360 computer and a "best fit" obtained using a least squares method. The Hall mobilities given by equation 23 were obtained in a similar way. A "best fit" was obtained to the relation

$$\mu_H = d + cB \qquad (26)$$

using the method of least squares. The constant d is then equal to the mobility in the limit of zero magnetic field.

There is observed to be a 12 percent spread in the values of ρ_{11} with the average of the three samples being 4.31 ohm-cm. The limit of instrument error is approximately $\pm$ 2 percent but the absolute accuracy is istimated to be $\pm$ 8 percent because of the uncertainty in the measurement of contact separation. The uncertainty is due to the fact that the mechanical and electrical center of the contacts are not

TABLE II

MEASURED VALUES OF THE GALVANOMAGNETIC COEFFICIENTS FOR ZnO AT ROOM TEMPERATURE (297°K)

Coefficient	Sample Number			
Resistivity	1A	1B	1C	2C
ρ_{11}	4.00	4.44	4.48	
ρ_{33}				4.89
Hall Mobility				
ρ_{213}/ρ_{11}	202	200	203	
ρ_{132}/ρ_{33}				183
Magnetoresistance Coefficient				
ρ_{1111}/ρ_{11} $(x10^{13})$	0.959	*	0.902	
ρ_{3333}/ρ_{33} $(x10^{13})$				0.836
ρ_{1122}/ρ_{11} $(x10^{13})$	5.28	4.86	4.96	
ρ_{1133}/ρ_{11} $(x10^{13})$	5.25	*	4.86	
ρ_{3311}/ρ_{33} $(x10^{13})$				4.11
ρ_{3322}/ρ_{33} $(x10^{13})$				4.28

The resistivities are in ohm-cm., the Hall mobilities are in cm^2/V-sec., and the magnetoresistance coefficients are in cm^4/V^2-$sec.^2$.

*See discussion in text.

necessarily coincident. These measurements demonstrate that the conductivity of ZnO is isotropic to within the experimental uncertainties of the order of 15 percent. Hutson's (13) measurement of the conductivity ratio ρ_{11}/ρ_{33}, inferred from microwave cavity losses, is in agreement with this result.

The magnetoresistance coefficient ρ_{3322}/ρ_{33} is equal to ρ_{3311}/ρ_{33} because of the symmetry of the material. The results of this redundant measurement was included in Table II to show the agreement with the symmetry predictions.

The Hall potential data of Figure 13 shows some scatter in the data points. This is due primarily to the presence of an induced emf which was not completely subtracted out by the bucking circuit. The induced emf is zero at peak magnetic field so that if one only plotted these peak field data points very little scatter in data is observed. The scatter in the Hall data for the other samples was much less than that which is observed for sample 1C. The larger induced emf was probably caused by a slight difference in the way the signal leads were twisted and routed to the sample.

The Hall mobility data of Table II shows that μ_H is approximately 200 $Cm^2/V\text{-sec}$. for all three type 1 samples. Seitz and Whitmore (9) made measurements on undoped samples having this same orientation and found μ_H = 200 $Cm^2/V\text{-sec}$ at room temperatures. They quote a value of 160 $Cm^2/V\text{-sec}$ for μ_H along the c-axis. This is about 10

percent lower than the corresponding value of 183 $Cm^2/V\text{-sec}$ shown in Table II. Hutson (12) shows a value of μ_H = 180 $Cm^2/V\text{-sec}$ at room temperature for measurements along the c-axis. These measurements show that the Hall constant $R_H = \mu_H \rho$ is very nearly isotropic with a value of 900 $Cm^3/Coulomb$. The measured sign of R_H indicates that the carriers are electrons. Carrier concentrations at room temperature can be calculated using the relation

$$n = \frac{\mu_H}{\mu} \frac{1}{R_H e} \tag{27}$$

with $\mu_H/\mu = 3\pi/8$ which is a good approximation for the experimental conditions. This calculation shows the carrier concentration to be approximately 8×10^{15} per cubic centimeter.

Figures 7 through 12 show the results of the magnetoresistance measurements. The ratio of transverse to longitudinal magnetoresistance is seen to be approximately five to one. The presence of a longitudinal magnetoresistance was checked further by taking magnetoresistance data as a function of angle. An approximate sinusoidal variation was observed as the sample was rotated from the transverse through the longitudinal position with a definite minimum value occurring at the longitudinal position.

There is very little published magnetoresistance data with which to compare the results of these measurements. No measurements have been made at high magnetic fields. Hutson (13) made some magnetoresistance measurements on a

c-axis single crystal in a DC magnetic field of 15.6 kilogauss. His data shows a value of $\Delta\rho/\rho$ 7×10^{-5}. .Assuming the magnetoresistance to follow a B^2 dependence, Figure 9 yields a value of $\Delta\rho/\rho$ 10^{-4} at 15.6 kilogauss. The two measurements are, therefore, in reasonable agreement.

When making magnetoresistance measurements on sample 1B it was observed that a large component of potential δV_{0I0B} was present on the probes. When the sample was orientated to measure the coefficient ρ_{1133} the ratio $\delta V_{0I0B}/\delta V_{0IEB} \simeq 10/1$. When the sample was then rotated 90 degrees to measure the coefficient ρ_{1122} the ratio dropped to $\delta V_{0I0B}/\delta V_{0IEB} \simeq 1/3$. These ratios were measured at a magnetic field strength of 20 kilogauss. The ratio became quite large again when the sample was orientated for the ρ_{1111} coefficient. The signal was so small for this orientation, however, that no accurate measurement of the ratio could be obtained. A longitudinal carrier concentration gradient is believed to be the cause of this effect. Bate and Beer (28) have considered the case of an exponential longitudinal gradient and make some predictions of results very similar to the results described above.

An attempt was made to measure the resistivity as a function of the length but the small size of the sample and relatively large probes made it impractical to make accurate measurements. A different measuring technique is required to detect carrier concentration gradients of this magnitude.

CHAPTER IV

INTERPRETATION OF RESULTS

Development of a Model

The model chosen to explain the conduction band processes must be in agreement with other types of experimental measurements made on ZnO as well as the galvanomagnetic measurements of this study. Some of the optical studies on ZnO suggest that a single ellipsoidal energy band centered at k = 0 yields a satisfactory explanation for the observed experimental measurements (15). We will proceed then to apply this model to the conduction processes and compare its predictions with the observed measurements.

A simple conduction band which exhibits the hexagonal symmetry of the crystal lattice is a single valley, centered at k = 0, which has an ellipsoid of revolution as a surface of constant energy. The axes of this ellipsoid must be parallel to the axes of the unit cell in order to exhibit the required hexagonal symmetry. The energy of an electron is then given by

$$\mathcal{E}(k) = \frac{\hbar^2}{2}\left[\frac{k_1^2}{m_{11}} + \frac{k_2^2}{m_{22}} + \frac{k_3^2}{m_{33}}\right] \qquad (28)$$

where k_1, k_2, and k_3 are the components of the wave number vector of the electron and m_{11}, m_{22}, and m_{33} are the components of the effective mass tensor which is diagonal in this coordinate system. It is assumed that a relaxation time exists and that it is a tensor with components which are a function of electron energy only. It is further assumed that the relaxation time is diagonal in the same coordinate system as the effective mass.

A theory of galvanomagnetic effects in a solid based on an energy band model as described above has been developed by Ables and Meiboom (26). The basic assumptions made in the development of the theory are: (a) The Boltzman transport equation with the relaxation time approximation is valid, (b) The relaxation time is isotropic and a function of energy only, (c) The energy of an electron can be approximated by a quadratic function of momentum near each extremum. Herring and Vogt (27) extended this theory to include a more general case where the relaxation time τ is anisotropic. They have shown that the effect is to weigh each component of the effective mass tensor, as it appears in the usual theory, with the reciprical of the corresponding component of the relaxation time tensor. Their result combined with the derivations of Ables and Meiboom allows one to write out the conductivity coefficients as follows:

$$\sigma_{\alpha\beta}(0) = (ne^2/m_{\alpha\alpha}) \left\langle \tau_{\alpha\alpha} \right\rangle \delta_{\alpha\beta} , \tag{29}$$

$$\sigma_{\alpha\beta\gamma}(\vec{B}) = (n|e|^3/m_{\alpha\alpha}m_{\beta\beta}) \left\langle \tau_{\alpha\alpha}\tau_{\beta\beta} \right\rangle \epsilon_{\alpha\beta\gamma} \tag{30}$$

$$\sigma_{\alpha\beta\gamma\delta}(\vec{B}) = (n|e|^4/m_{\alpha\alpha}m_{\beta\beta}) \times$$

$$\sum_{\lambda} \frac{1}{2m_{\lambda\lambda}} (\epsilon_{\alpha\gamma\lambda}\epsilon_{\lambda\delta\beta} + \epsilon_{\alpha\delta\lambda}\epsilon_{\lambda\delta\beta}) \langle \tau_{\alpha\alpha}\tau_{\beta\beta}\tau_{\lambda\lambda} \rangle \qquad (31)$$

where the average, $\langle \phi(\mathcal{E}) \rangle$, for a function of energy, $\phi(\mathcal{E})$, is defined by the relation:

$$\langle \phi(\mathcal{E}) \rangle = -\frac{2}{3} \frac{\int_0^\infty \phi(\mathcal{E})\, \mathcal{E}^{3/2} (\partial f^o/\partial \mathcal{E}) d\mathcal{E}}{\int_0^\infty \mathcal{E}^{\frac{1}{2}} f^o d\mathcal{E}} , \qquad (32)$$

f^o is the Fermi-Dirac distribution function, n is the volume density of electrons, e is the charge of an electron and $\epsilon_{\alpha\beta\gamma}$ is a permutation symbol defined by

$$\epsilon_{\alpha\beta\gamma} = \begin{array}{l} +1 \text{ if } \alpha\beta\gamma \text{ is an even permutation} \\ -1 \text{ if } \alpha\beta\gamma \text{ is an odd permutation} \\ 0 \text{ otherwise, that is, if two or more of the indices are the same.} \end{array} \qquad (33)$$

Using the inversion formulas, the following expressions are obtained for the galvanomagnetic coefficients:

$$\rho_{\alpha\beta}(0) = (m_{\alpha\alpha}/n|e|^2 \langle \tau_{\alpha\alpha} \rangle)\delta_{\alpha\beta} \qquad (34)$$

$$\rho_{\alpha\beta\gamma}(\vec{B}) = \frac{1}{n|e|} \frac{\langle \tau_{\alpha\alpha}\tau_{\beta\beta} \rangle}{\langle \tau_{\alpha\alpha} \rangle \langle \tau_{\beta\beta} \rangle} \epsilon_{\alpha\beta\gamma} \qquad (35)$$

$$\rho_{\alpha\alpha\alpha\alpha}(\vec{B}) = 0 \qquad (36)$$

$$\rho_{\alpha\alpha\beta\beta}(\vec{B}) = \frac{1}{nm_{\gamma\gamma}} \left[\frac{\langle \tau_{\alpha\alpha}^2 \tau_{\gamma\gamma} \rangle}{\langle \tau_{\alpha\alpha} \rangle} - \frac{\langle \tau_{\alpha\alpha}\tau_{\gamma\gamma} \rangle^2}{\langle \tau_{\alpha\alpha} \rangle^2 \langle \tau_{\gamma\gamma} \rangle} \right] \qquad (37)$$

$$\rho_{\alpha\beta\alpha\beta}(\vec{B}) = -\frac{1}{2m m_{\gamma\gamma}} \left[\frac{\langle \tau_{\alpha\alpha}\tau_{\beta\beta}\tau_{\gamma\gamma} \rangle}{\langle \tau_{\alpha\alpha} \rangle \langle \tau_{\beta\beta} \rangle} - \frac{\langle \tau_{\alpha\alpha}\tau_{\gamma\gamma} \rangle \langle \tau_{\beta\beta}\tau_{\gamma\gamma} \rangle}{\langle \tau_{\alpha\alpha} \rangle \langle \tau_{\beta\beta} \rangle \langle \tau_{\gamma\gamma} \rangle} \right] \qquad (38)$$

Unless required by the Kronecker delta, $\delta_{\alpha\beta}$, $\alpha \neq \beta \neq \gamma$ and can be assigned according to any of the six permutations of 1, 2, and 3. With these expressions for the coefficients at hand we now proceed to compare the experimental results with the predictions for this model.

Resistivity at Zero Magnetic Field

Due to symmetry there are only two independent resistivity coefficients and $\rho_{11} = \rho_{22}$. Table II shows some variation in the measured values of the resistivity but it is concluded that the resistivity of ZnO is isotropic since the spread in values is less than the experimental uncertainty of $\pm$ 8 percent. The predicted resistivity for this model is given by equation 34 which shows that if a small amount of anisotropies exists it could be due to the effective masses, the relaxation times, or a combination of the two.

Hall Effect

The measurements of Table II indicate that the Hall constant, $R_H = \mu_H \rho$, is very nearly isotropic with a value of 900 cm^3/coulomb. The two independent coefficients are, according to the predictions of equation 35:

$$R_H = \rho_{213} = -\frac{1}{n|e|} \frac{\langle \tau_{22} \tau_{11} \rangle}{\langle \tau_{22} \rangle \langle \tau_{11} \rangle} \tag{39}$$

$$R_H = \rho_{132} = -\frac{1}{n|e|} \frac{\langle \tau_{11} \tau_{33} \rangle}{\langle \tau_{11} \rangle \langle \tau_{33} \rangle} \tag{40}$$

It is observed then that the form of the relaxation time determines whether the predicted Hall coefficient is isotropic or not. The model was developed assuming an anisotropic relaxation time of the form (call this type form I):

$$\text{I} \qquad \tau_{ij} = \tau_i(\mathcal{E})\, \delta_{ij} \tag{41}$$

There are other forms for the relaxation that should be considered, for example

II An anisotropic relaxation time with a common energy dependence:

$$\tau_{ij} = \tau_i\, \phi(\mathcal{E})\, \delta_{ij} \tag{42}$$

III An isotropic relaxation which is a function of energy

$$\tau_{ij} = \phi(\mathcal{E})\, \delta_{ij} \tag{43}$$

IV An anisotropic constant relaxation time

$$\tau_{ij} = \tau_i\, \delta_{ij} \tag{44}$$

V An isotropic constant relaxation time:

$$\tau_{ij} = \tau\, \delta_{ij} \tag{45}$$

All forms of the relaxation except I predict an isotropic Hall coefficient.

Magnetoresistance

An analysis of the transverse magnetoresistance results is begun by substituting the various forms for relaxation time given by equations 41 through 45 into equations 37 and 38. Choosing a constant relaxation time of

the form IV or V yields a prediction of zero transverse magnetoresistance. These forms of the relaxation time are therefore rejected since they are in gross disagreement with the measured results. Looking at Table II, the measured results show that to a close approximation

$$\frac{\rho_{3311}}{\rho_{33}} = \frac{\rho_{3322}}{\rho_{33}} \tag{46}$$

$$\frac{\rho_{1122}}{\rho_{11}} = \frac{\rho_{1133}}{\rho_{11}} \tag{47}$$

and within the limits of a measurement of error $\pm$ 10 percent it is observed that

$$\frac{\rho_{1122}}{\rho_{11}} = \frac{\rho_{3311}}{\rho_{33}} \tag{48}$$

The equality of equation 46 is predicted by symmetry. The results of measurement given in Table II show that the two quantities differ by less than 4 percent. This agreement is gratifying and generates confidence in the measurement and techniques used.

Using the results of equation 34 and 37, equation 47 requires that

$$\frac{|e|^2 \langle \tau_{11} \rangle}{m_{11} m_{33}} \left[\frac{\langle \tau_{11}^2 \tau_{33} \rangle}{\langle \tau_{11} \rangle^2} - \frac{\langle \tau_{11} \tau_{33} \rangle^2}{\langle \tau_{11} \rangle^2 \langle \tau_{33} \rangle} \right]$$

$$= \frac{|e|^2 \langle \tau_{22} \rangle}{m_{11} m_{22}} \left[\frac{\langle \tau_{11}^2 \tau_{22} \rangle}{\langle \tau_{11} \rangle^2} - \frac{\langle \tau_{11} \tau_{22} \rangle^2}{\langle \tau_{11} \rangle^2 \langle \tau_{22} \rangle} \right] . \tag{49}$$

This is not true in general for relaxation times of form I.

Relaxation time of form II would satisfy the equality provided that the effective mass were isotropic.

In like manner, substituting into equation 48 requires that

$$\frac{|e|^2 \langle \tau_{11} \rangle}{m_{11} m_{33}} \left[\frac{\langle \tau_{11}^2 \tau_{33} \rangle}{\langle \tau_{11} \rangle^2} - \frac{\langle \tau_{11} \tau_{33} \rangle^2}{\langle \tau_{11} \rangle^2 \langle \tau_{33} \rangle} \right]$$

$$= \frac{|e|^2 \langle \tau_{33} \rangle}{m_{33} m_{22}} \left[\frac{\langle \tau_{33}^2 \tau_{22} \rangle}{\langle \tau_{33} \rangle^2} - \frac{\langle \tau_{33} \tau_{22} \rangle^2}{\langle \tau_{33} \rangle^2 \langle \tau_{22} \rangle} \right] \qquad (50)$$

This also is not true in general for relaxation times of form I but, since $m_{11} = m_{22}$ and $\tau_{11} = \tau_{22}$ by symmetry, this relaxation is satisfied by the relaxation times of form II through V.

As shown by Table II, the longitudinal magnetoresistance is not large but is definitely non zero. The ratio of transverse to longitudinal magnetoresistance is approximately 5/1. The presence of a non zero longitudinal magnetoresistance is one of the main factors which has caused other investigators to choose a "many valley" model as opposed to a single ellipsoid model (13). Other experimental evidence, however, strongly supports a single ellipsoid model (15). The most logical solution, therefore, is to propose some slight modification to the single ellipsoidal model which could account for the observed longitudinal magnetoresistance. A slight warping of the energy surface due to higher bands has been suggested and appears to be a logical proposal (14). A small amount of

warping would introduce enough assymetry to the surface to produce a measurable longitudinal magnetoresistance.

The possibility of a carrier concentration gradient in the sample should not be overlooked as a source or partial source for the observed longitudinal magnetoresistance. Bate and Beer (28) have shown that a carrier concentration in the sample can produce a measurable longitudinal magnetoresistance. Some sections of the crystal from which the samples were cut did show a measurable gradient, however, the change in resistivity of the samples herein reported was ≤ 8 percent along the length of the sample. The sample size and probe size restricted the accuracy of this measurement to this value. It is worth noting, however, that the ratio of transverse to longitudinal magnetoresistance of 5/1 for the c-axis crystal sample is in close agreement with Hutson's value of approximately 6/1. The crystal samples of this study and those of Hutson's were grown using a vapor reaction process. It is possible that this growth process introduces a characteristic gradient in the crystals. The effect of or reduction of carrier concentration gradients should be thoroughly investigated in future galvanomagnetic studies of ZnO. It is suggested that the effects described on page 52 of this report be used to select usable samples from a group for the purpose of making galvanomagnetic measurements.

Discussion of the Single Ellipsoid Model

The above evidence narrows the choice of relaxation time to either form III, an isotropic function of energy, or of form II, an anisotropic relaxation time with a factorable energy dependence. Since III is a special case of II the assumption is made for the rest of the analysis that the relaxation time is of form II.

A combination of equations 34, 35, and 37 yields the general results:

$$\rho_{\alpha\beta} = \frac{1}{n|e|\langle\mu_\alpha\rangle}\delta_{\alpha\beta} \tag{51}$$

$$\frac{\rho_{\alpha\beta\gamma}}{\rho_{\alpha\beta}} = (\mu_H)_{\alpha\alpha} = \langle\mu_\alpha\rangle\left[\frac{\langle\phi(\mathcal{E})^2\rangle}{\langle\phi(\mathcal{E})\rangle^2}\right] \tag{52}$$

$$\frac{\rho_{\alpha\alpha\beta\beta}}{\rho_{\alpha\alpha}} = \langle\mu_\alpha\rangle\langle\mu_\gamma\rangle\left[\frac{\langle\phi(\mathcal{E})^3\rangle\langle\phi(\mathcal{E})\rangle - \langle\phi(\mathcal{E})^2\rangle^2}{\langle\phi(\mathcal{E})\rangle^4}\right] \tag{53}$$

where the drift mobility is given by

$$\mu_\alpha = \frac{|e|\,\tau_{\alpha\alpha}}{m_{\alpha\alpha}} \tag{54}$$

These equations may be further simplified by letting

$$A = \frac{\langle\phi(\mathcal{E})^2\rangle}{\langle\phi(\mathcal{E})\rangle^2} \tag{55}$$

$$B = \frac{\langle\phi(\mathcal{E})^3\rangle\langle\phi(\mathcal{E})\rangle - \langle\phi(\mathcal{E})^2\rangle^2}{\langle\phi(\mathcal{E})\rangle^4} \tag{56}$$

These equations have been used to derive the galvanomagnetic coefficients for this model. The results are presented in Table III. Neglecting the longitudinal magnetoresistance

TABLE III

GALVANOMAGNETIC COEFFICIENTS OF A SINGLE ELLIPSOID MODEL OF THE ENERGY SURFACES IN ZnO COMPARED TO THE EXPERIMENTALLY MEASURED VALUES

Galvanomagnetic Coefficients	Derived Expression	Measured Values*
ρ_{11}	$1/n\|e\|\langle\mu_1\rangle$	4.31 Ohm cm
ρ_{33}	$1/n\|e\|\langle\mu_3\rangle$	4.89 Ohm cm
ρ_{213}/ρ_{11}	$A\langle\mu_1\rangle$	$202\frac{Cm^2}{V\ sec.}$
ρ_{132}/ρ_{33}	$A\langle\mu_3\rangle$	$183\frac{Cm^2}{V\ sec.}$
ρ_{1111}/ρ_{11}	0	$0.930 \times 10^{-13}\frac{Cm^4}{V^2 sec^2}$
ρ_{3333}/ρ_{33}	0	0.836×10^{-13} "
ρ_{1122}/ρ_{11}	$B\langle\mu_1\rangle\langle\mu_3\rangle$	5.03×10^{-13} "
ρ_{1133}/ρ_{11}	$B\langle\mu_1\rangle^2$	5.05×10^{-13} "
ρ_{3311}/ρ_{33}	$B\langle\mu_1\rangle\langle\mu_3\rangle$	4.11×10^{-13} "
ρ_{3322}/ρ_{33}	$B\langle\mu_1\rangle\langle\mu_3\rangle$	4.28×10^{-13} "

*Average values for the samples measured.

results, a comparison of the measured data and the theoretical expressions in Table III show that the data fits the single ellipsoid model within experimental error.

One characteristic indicated in Table III is a low value of the ratio μ_1/μ_3 (on the order of 1.1). An accurate value is difficult to determine since there is a variation in resistivity from sample to sample. Optical and thermal studies by other investigators suggest that the effective mass is nearly isotropic (12) (13) (14) (15). This low value of μ_1/μ_3 obtained from these galvanomagnetic studies, therefore, indicates that the anisotropy of the scattering time is very small.

Neither of the parameters A or B of equations 55 and 56 can be determined from glavanomagnetic measurements. They both depend on the way in which the averages are taken. The parameter A is equal to the ratio of Hall mobility to drift mobility and is very close to unity for all known scattering mechanisms. For acoustic mode scattering it has a value of $3\pi/8$.

About the only remaining way to add validity to the choice of a single ellipsoid model would be to compare the the magnitude of the measured coefficients with the calculated values predicted by theory. After considerable investigation, this approach was discontinued. The problem with this approach is that all the parameters required in the theory may not have been measured and the accuracy of some that have been measured is unknown or questionable.

For example, in pursuing this approach, it was found that in many cases the parameters such as piezoelectric constants, elastic constants, and dielectric constants (all tensor quantities) were averaged. The scattering theory in which they were used is then essentially an isotropic theory. With the multitude of parameters available a satisfactory fit could be obtained, but any predicted anisotropy of relaxation time or mobility would be questionable.

Summary and Conclusion

The galvanomagnetic coefficients of ZnO single crystal specimens have been measured at room temperature using pulsed magnetic fields up to 200 kilogauss. Even at these field strengths, the relation $\mu B \equiv \omega\tau < 1$ is satisfied, therefore, the measurements and analysis of the galvanomagnetic effects was done using a phenomenological approach. Onsager's relations and the symmetry requirements of the material were used to identify the independent non zero coefficients and to define the crystal orientations best suited to the experiment. Only two crystals with orthogonal axes were required to evaluate the 10 independent coefficients.

The results of the measurements showed that the Hall constant, $R_H = \mu_H \rho$, was isotropic within the limits of experimental error and had a value of approximately 900 cm^3/coulomb.

Both transverse and longitudinal magnetoresistance

followed a simple B^2 magnetic field dependence. The ratio of transverse to longitudinal magnetoresistance was found to be approximately 5/1 for both orientations of the current axes.

Except for the observance of a non zero longitudinal magnetoresistance, the experimentally observed results of the galvanomagnetic measurements are shown to be in good agreement with a model for the conduction band conduction processes which assumes that the conduction band is composed of a single valley which is parabolic in $\vec{k}$ and has an ellipsoid of revolution for surfaces of constant energy. The relaxation time was assumed to be of the form $\tau_{\alpha\beta} = \tau_\alpha \phi(\mathcal{E}) \delta_{\alpha\beta}$. The longitudinal magnetoresistance was attributed primarily to a small carrier concentration gradient in the samples. Other possible sources are warping of the energy surfaces from higher band and a small amount of misalignment of the sample axes.

BIBLIOGRAPHY

1. Cambell, L. L. Galvanomagnetic and Thermomagnetic Effects. New York: Longmanns, Green and Co., 1923.

2. Glicksman, M. "The Magnetoresistivity of Germanium and Silicon." Progress in Semiconductors, Vol. 3, ed. A. F. Gibson, R. E. Burgess, and P. A. Aigrain. New York: J. Wiley and Sons, Inc., 1958.

3. Beer, A. C. "Galvanomagnetic Effects in Semiconductors." Solid State Physics, ed. Frederick Seitz and David Turnbull. New York: Academic Press Inc., Supplement 4, 1963.

4. Becker, W. A. "Band Characteristics near Principal Minima from Magnetoresistance." Semiconductors and Semimetals, Vol. 1, ed. R. K. Willardson and A. C. Beer. New York: Academic Press Inc., 1966.

5. Ray, B. II-VI Compounds. New York: Pergamon Press, 1969.

6. Glasser, M. L. "Symmetry Properties of the Wurtzite Structure." J. Phys. Chem. Solids, 10, 229 (1959).

7. Brown, H. E. Zinc Oxide Rediscovered. New York: New Jersey Zinc Co. 1957.

8. Gieland, G., E. Mollwa and F. Stockman. "Electronic Processes in Zinc Oxide." Solid State Physics, Vol. 8, ed. Frederick Seitz and David Turnbull. New York: Academic Press Inc., 1959.

9. Seitz, M. A. and D. H. Whitmore. "Electronic Drift Mobilities and Space-Charge-Limited Currents in Lithium-Doped Zinc Oxide." J. Phys. Chem. Solids, 8, 1033 (1968).

10. Harrison, S. E. "Conductivity and Hall-Effect of ZnO at Low Temperatures." Phys. Rev., 93, 52 (1954).

11. Bogner, G. "Measurements of the Electrical Conductivity and Hall Effect on ZnO Crystals." J. Phys. Chem. Solids, 19, 235 (1961)

12. Hutson, A. R. "Hall Effect Studies of Doped Zinc Oxide Single Crystals." Phys. Rev., 108, 222 (1957).

13. Hutson, A. R. "Electronic Properties of ZnO." J. Phys. Chem. Solids, 108, 467 (1959).

14. Hutson, A. R. "Piezoelectric Scattering and Phonon Drag in ZnO and CdS." J. Appl. Phys., 32, 2287 (1961).

15. Dietz, R. E., J. J. Hopfield, and D. G. Thomas. "Excitons and the Absorption Edge of ZnO." J. Appl. Phys., 32, 2282 (1961).

16. Smith, A. C., J. F. Janak, and R. B. Adler. Electronic Conduction in Solids. New York: McGraw-Hill Book Co., 1967.

17. Kao, L. P., and E. Katz. "Phenomenological Theory of Anisotropic Isothermal Galvanomagnetic Effects." J. Phys. Chem. Solids, 6, 223 (1958).

18. Watanabe, H., M. Wada, and T. Takahashi. "Optical and Electrical Properties of ZnO Crystals." Japanese J. Appl. Phys., 3, 617(1964).

19. Weiss, H. "Magnetoresistance." Semiconductors and Semimetals, ed. R. F. Willardson and A. C. Beer. (Academic Press, New York, 1966), Vol. 1, Chapter 10, P. 315.

20. Thomas, D. G. "Interstitial Zinc in Zinc Oxide." J. Phys. Chem. Solids, 3, 229 (1957).

21. Aven, M. and R. K. Swank. "Ohmic Contacts to Wide-Band Gap Semiconductors." Ohmic Contacts to Semiconductors, ed. Bertram Schwartz. (Electro-Chemical Society Inc., New York, 1969).

22. Russell, K. J. and W. J. Leivo. "Pulsed Magnet System for Production of High Magnetic Fields." Proc. Okla. Acad. Sci., 46, 122 (1966).

23. Laskowski, L. B. "An Investigation of the Transport Properties of Holes in a Semiconducting Diamond." (Unpub. Ph.D. Dissertation, Oklahoma State University, 1972).

24. Montgomery, D. B. Solenoid Magnet Design. (Wiley Interscience, a Division of John Wiley and Sons, New York, 1969).

25. Kapitza, P. Collected Papers of P. L. Kapitza. Ed. D. ter Haar. Oxford, New York, Pergamon Press, 1964-1967, 3 volumes.

26. Ables, B. and S. Meiboom. "Theory of the Galvanomagnetic Effects in Germanium." Phys. Rev., 95, 31 (1954).

27. Herring, C. and E. Vogt. "Transport and Deformation-Potential Theory for Many-Valley Semiconductors with Anisotropic Scattering." Phys. Rev., 101, 944 (1956).

28. Bate, R. T. and A. C. Beer. "Influence of Conductivity Gradients on Galvanomagnetic Effects in Semiconductors." J. Appl. Phys., 32, 800 (1961).

VITA

Walter Claud Rhodes, Jr.

Candidate for the Degree of

Doctor of Philosophy

Thesis: PULSED FIELD GALVANOMAGNETIC MEASUREMENTS ON ZINC OXIDE

Major Field: Physics

Biographical:

Personal Data: Born in Tipton, Oklahoma, November 3, 1930, the son of Mr. and Mrs. Walter Rhodes.

Education: Graduated from Snyder High School, Snyder, Oklahoma in May 1948; received the Bachelor of Science degree in Physics from Central State University in 1957; attended University of Oklahoma in Spring of 1957; received the Master of Science degree in Physics from Oklahoma State University in May, 1968; completed requirements for the Doctor of Philosophy degree at Oklahoma State University in July, 1973.

Professional Experience: Radio Mechanics School and Radio Maintenance, U.S. Air force, 1950-54; graduate teaching assistant, Oklahoma University 1957; Senior Electronics Engineer, Melpar, Inc., Falls Church, Virginia, 1957-60; Director Range Instrumentation Lab., Keltec Industries, Alexandria, Virginia, 1960-65; graduate teaching assistant, Oklahoma State University, 1965-72.